CHAPTER 8

Titan's weather, climate, and paleoclimate

Juan M. Lora[a], Elizabeth P. Turtle[b], and Jonathan L. Mitchell[c,d]

[a]*Department of Earth and Planetary Sciences, Yale University, New Haven, CT, United States* [b]*The Johns Hopkins University Applied Physics Laboratory, Laurel, MD, United States* [c]*Department of Earth, Planetary, and Space Sciences, University of California Los Angeles, Los Angeles, CA, United States* [d]*Department of Atmospheric and Oceanic Sciences, University of California Los Angeles, Los Angeles, CA, United States*

1 Introduction

Titan is the only satellite in the solar system with a massive atmosphere. Titan is also the only terrestrial body, outside of Earth, known to support an active hydrologic cycle complete with precipitation, surface hydrology, and stable surface liquids (e.g., Lunine and Atreya, 2008; Lunine and Lorenz, 2009; Mitchell and Lora, 2016; Hayes et al., 2018). This makes it a fascinating target for study, yet much of our knowledge of the lower atmosphere and its behavior is recent, in part because the surface and lower atmosphere are entirely obscured by Titan's haze. Prior to the *Voyager* missions, even the bulk composition of Titan's atmosphere was unknown—methane had been discovered spectroscopically (Kuiper, 1944), but the nitrogen remained undetected. *Voyager 1* measured Titan's surface pressure and temperature, providing evidence of a subsaturated near-surface environment (Lindal et al., 1983) as well as showing unequivocally that methane exists near its triple point within a nitrogen atmosphere (e.g., Broadfoot et al., 1981). The surface itself was not revealed for roughly another decade, and its nature remained unknown until *Cassini-Huygens*.

Investigations of Titan in the decades between *Voyager* and *Cassini* yielded several insights into the possible operation of its climate system. Given the presence of methane and its photochemical conversion to ethane in the upper atmosphere (Strobel, 1974; Yung et al., 1984), a strong early prediction was that Titan would host a global methane–ethane ocean (Lunine et al., 1983); however, subsequent observations of the surface showed this not to be the case (Muhleman et al., 1990; Smith et al., 1996). On the other hand, tentative expectations of active weather (e.g., Toon et al., 1988; Lorenz, 1993; Awal and Lunine, 1994) were spectacularly confirmed by observations of tropospheric cloud outbursts with ground-based observations:

Titan After Cassini-Huygens. https://doi.org/10.1016/B978-0-323-99161-2.00002-4

First, disk-integrated spectra were used to detect sporadic, and evolving, cloud coverage (Griffith et al., 1998, 2000); later, adaptive optics enabled direct imaging of clouds at Titan's south pole (Brown et al., 2002; Roe et al., 2002). These observations occurred close to Titan's southern summer solstice and, combined with the obviously transient nature of the clouds, strongly indicated a seasonal convective origin for Titan's cloudiness.

In addition to progress with theory and observations, an important tool emerged in the decades between *Voyager* and *Cassini* with which to probe the characteristics of Titan's atmosphere: numerical general circulation models (GCMs). Initially, most investigations with such models concentrated on the dynamics of the middle atmosphere (e.g., Hourdin et al., 1995), but subsequent studies also investigated the methane cycle and near-surface environments (e.g., Tokano, 2005; Mitchell et al., 2006; Rannou et al., 2006). Many early such studies used idealized assumptions and simplifications, but the latest generation models are three dimensional and increasingly comprehensive (Lora et al., 2019); thus, they are crucial tools (see Lebonnois et al., 2014) that give context to piecemeal observations of the weather, allow quantitative evaluation of climate processes, and provide predictions for future study.

The *Cassini–Huygens* mission enabled huge progress in our understanding of Titan's climate system by providing ground truth via in situ measurements of several vital aspects of Titan's equatorial environment, by making a multitude of unanticipated discoveries, and by monitoring the seasonal evolution from northern winter (2004–2009) through northern summer solstice (in 2017), in addition to stimulating modeling studies. Numerous mysteries were decisively resolved early on, like the presence of polar liquids (Stofan et al., 2007), while other results—for instance, the seasonal distribution of clouds (Turtle et al., 2018)—were teased out over the course of the mission. All of these insights have permitted an extensive and increasingly self-consistent—if yet incomplete—picture of this unique climate system and its role within the larger Titan context (see also MacKenzie et al., 2021).

In this chapter, we review the state of knowledge of Titan's climate system, from weather processes to the long-term climate evolution, with particular attention to advances made during and after the *Cassini* Solstice Mission (2010–2017), building on earlier reviews by numerous authors (Lunine and Lorenz, 2009; Roe, 2012; Griffith et al., 2014; Lebonnois et al., 2014; Mitchell and Lora, 2016; Hörst, 2017; Hayes et al., 2018). Much of the focus is on the interactions between the atmosphere and the surface, as it is these interactions that enable Titan's seasonal weather and climate, and our understanding of them has improved considerably. We begin by examining the weather observed by *Cassini–Huygens* and what it reveals about Titan as a system and the processes that dominate it. We also consider Titan's climate, the statistical description of the state of the atmosphere–surface system, including its seasonally evolving averages and what we have learned about variability. Finally, we review hypotheses about the past evolution of Titan's climate, and whether previous climate states may be reflected by geologic archives on its surface.

2 *Two seasons of weather from* Cassini–Huygens

2.1 *Observed environment of the lower atmosphere*

At lower latitudes, the thermal structure of Titan's lower atmosphere is largely set by radiative processes. As a result of its high density ($\sim$1–5 kg m^{-3}) and cool temperatures ($\sim$70–90 K) (Fulchignoni et al., 2005), this region below 50 km altitude responds on timescales that are long relative to the variations of insolation; estimates of the radiative relaxation times vary, but range between about one Titan season—roughly seven Earth years—to longer than a Titan year (Strobel et al., 2009; Bézard et al., 2018). Either way, these long timescales suggest little seasonal variation, and this is indeed what has been observed (e.g., Flasar et al., 2014).

Retrieved and in situ measurements of the atmospheric temperature from *Voyager*, *Cassini*, and *Huygens* agree well with each other and therefore imply that, especially between roughly 5 and 20 km in altitude, there is almost no variation globally (Fig. 1), meaning that seasonal contrasts are entirely absent (Lindal et al., 1983; Schinder et al., 2011, 2012, 2020; Fulchignoni et al.,

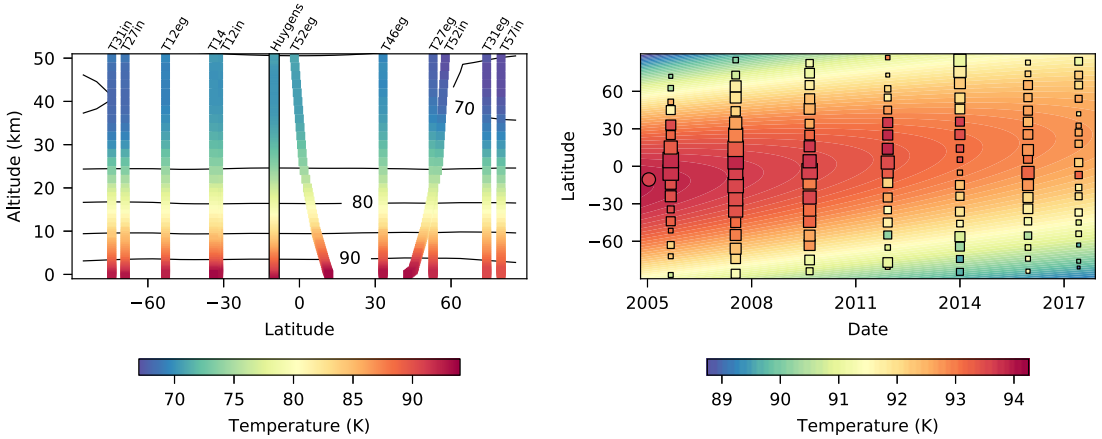

Fig. 1

Observed and simulated temperatures. *Left*: Atmospheric temperatures during northern winter derived from *Cassini* radio occultations (Schinder et al., 2011, 2012, 2020) and measured by *Huygens* (Fulchignoni et al., 2005) (*colors*, labels at the top; "in" and "eg" refer to "ingress" and "egress," respectively). *Black contours* show corresponding temperatures from a recent GCM simulation (Lora et al., 2022). *Right*: Retrieved surface brightness temperatures (*squares*) (Jennings et al., 2019) and in situ measurement of surface temperature (*circle*) (Fulchignoni et al., 2005) overlying the analytical estimate of Jennings et al. (2019) of the seasonal evolution fit to the brightness temperatures (*colors*). The dates used for the brightness temperatures correspond to the midpoints of the ranges in Jennings et al. (2019). The sizes of the squares are inversely proportional to their respective uncertainties in temperature.

2005). Latitudinal contrasts in this vertical region are also nearly nonexistent, implying that energy is effectively redistributed much faster than it is altered by radiation. At higher levels, high latitudes in both hemispheres have cooler temperatures than the low latitudes: Temperature retrievals from the southern hemisphere (up to 74°S) during its summer show that the broad temperature minimum region (30–50 km altitude) was 2–3 K cooler than at lower latitudes, while the corresponding mid- to late-winter temperatures of the northern hemisphere (up to 80°N) were up to 4 K cooler, with a more pronounced temperature minimum of 66 K occurring at around 50 km altitude. These are still modest contrasts relative to what would be expected from purely radiative equilibrium, indicating that dynamical heating is an important process in Titan's atmosphere; GCM simulations also nicely reproduce all of these characteristics (Fig. 1).

Below ~5 km, measured temperature variations with latitude are more pronounced—though still small—meaning that surface–atmosphere coupling and a surface with relatively low thermal inertia play important roles in setting the thermal structure of these layers. In fact, all measured profiles at lower latitudes agree well and indicate lapse rates that are close to dry adiabatic especially in the lowermost 2 km, implying that convective mixing occurs (Lindal et al., 1983; Fulchignoni et al., 2005; Griffith et al., 2008; Schinder et al., 2011). They also agree with the surface temperature of 93.7 K measured in situ (Fulchignoni et al., 2005). At higher latitudes, the vertical temperature gradients are less steep, meaning that near-surface temperatures are lower but also that these profiles are more stable. Toward the late-summer south pole, near-surface temperatures retrieved from *Cassini* measurements decreased to around 92 K; near the late-winter north pole, they were closer to 90 K (Schinder et al., 2012). Indeed, measured temperatures at the highest northern latitudes (74–80°N) were nearly isothermal in the lowest kilometer, reminiscent of polar inversions suggesting a negative energy balance at the surface due to polar night, and indicative of strongly stable near-surface air. Dry convection was therefore likely absent at these latitudes and times.

Importantly, the above temperatures from radio occultations agree remarkably well with surface brightness temperatures derived from radiances in the thermal infrared measured by *Cassini* (e.g., Jennings et al., 2011). Given that they cover nearly the full transition from northern winter solstice to summer solstice, these data provide particular insight into the evolution of the near-surface environment. A few assumptions are necessary, including a surface emissivity of unity at 19 μm (the agreement between surface brightness temperatures and near-surface temperatures from occultations suggests this is a good assumption) and that all longitudes at similar latitudes behave similarly (Jennings et al., 2009, 2019); nevertheless, the results provide a compelling illustration of significant seasonal variation in the near-surface environment (Fig. 1), despite the massive and cold overlying atmosphere. (Again, GCM results agree with the overall seasonal trends, albeit with some discrepancies that are likely due to the details of the surface; see Section 3.1).

In particular, the hottest region at the beginning of *Cassini* observations was near the location of the *Huygens* probe's landing at 10°S, but by the northern summer solstice in late 2017 it had migrated considerably into the northern hemisphere. This evolution roughly followed the subsolar point, with a small lag suggestive of a relatively low surface thermal inertia (Jennings et al., 2016, 2019; Janssen et al., 2016). Modest observed diurnal variations are also consistent with this (Cottini et al., 2012). Equator-to-pole temperature gradients were largest in the fall/winter hemisphere, but also decreased between southern summer and northern summer as a result of Saturn's orbital eccentricity, which takes Titan farther from the Sun during northern solstice and correspondingly leads to relative cooling of the lower latitudes. Thus, *Cassini* clearly observed seasonal variations of the surface temperatures, which correspond to variations of other fields that affect Titan's climate.

We next turn to the methane humidity. Despite the massive atmospheric methane inventory on Titan (roughly 5m of precipitable methane; Tokano et al., 2006), the humidity of Titan's lower atmosphere has been notoriously difficult to measure as a result of the high opacity. The in situ measurements made by *Huygens* show that, at 10°S during summer, the relative humidity between the temperature minimum around 40 km and roughly 5 km was near 100% and decreased to 50% at the surface, with the lowermost portion comprising a constant mole fraction indicative of mixing (Fig. 2) (Niemann et al., 2010). While crucial, this measurement

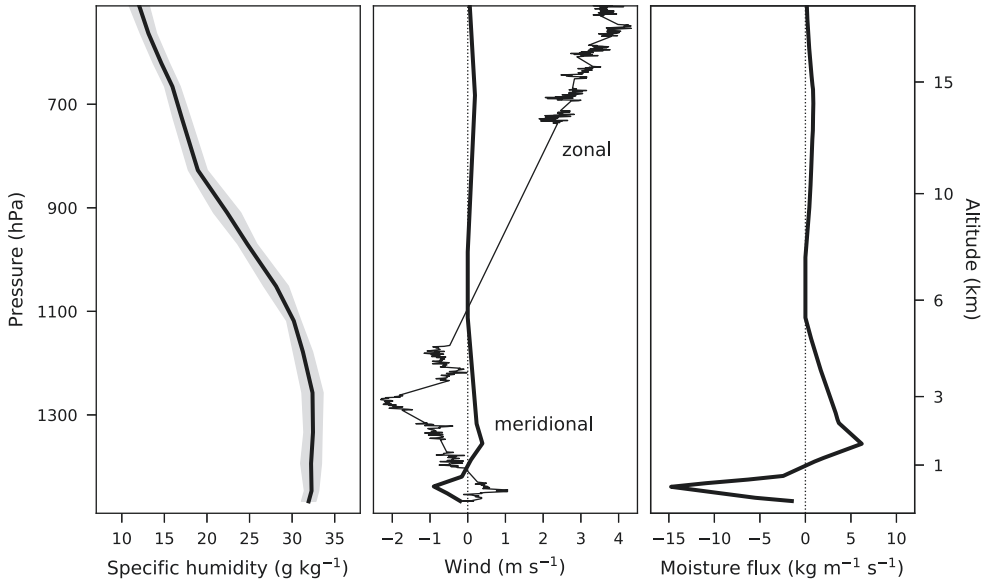

Fig. 2

Observed winds, humidity, and moisture transport. *Left*: Specific humidity of methane measured in situ during the *Huygens* descent, with standard deviation shown (Niemann et al., 2010). *Middle*: Zonal (*thin curve*) and meridional (*thick curve*) winds measured or inferred from *Huygens* (Bird et al., 2005; Karkoschka, 2016). *Right*: Profile of northward atmospheric moisture transport approximated using the observed profiles of humidity and meridional winds.

alone is difficult to interpret in the context of the larger methane cycle (i.e., Griffith et al., 2014; Mitchell and Lora, 2016): Is the near-equatorial near-surface humidity set by vapor pressure equilibrium with local liquids that are not pure methane (Tan et al., 2013), or by a global cycle controlled by equilibrium with polar surface liquids?

Some understanding of humidity variations with latitude can help answer this question. An initial estimate from ground-based observations of CH_3D (a less-abundant isotopologue of methane) suggested little latitudinal variation, but was limited to low latitudes (Penteado and Griffith, 2010). Subsequent ground-based, high-resolution observations, in combination with *Cassini* data, retrieved methane abundances during the northern spring that indicated an increase in tropospheric humidity toward the south pole (Ádámkovics et al., 2016). Finally, these latter observations were reinterpreted (using surface temperatures from the same season; Jennings et al., 2016) to estimate near-surface relative humidity variations (Lora and Ádámkovics, 2017). The results show a minimum humidity of around 50% between 15 and 30°N, and increases toward both poles (albeit with large uncertainties), with values consistent with 80% at southern mid-latitudes and 100% at the north pole (Fig. 3). These results have important implications for surface–atmosphere interactions and are discussed in further detail in Section 3.

These humidity estimates in fact suggest that large-scale atmospheric moisture transport is important, so observational constraints on the winds could further clarify the picture. Unfortunately, winds from the lower atmosphere are even more difficult to measure than humidity: Temperature retrievals are insufficient to determine the zonal wind field in balance with temperature gradients, as has been done for the middle atmosphere (Flasar et al., 2005; Achterberg et al., 2008, 2011), while trace constituents that can reveal the meridional circulation (e.g., Teanby et al., 2019; Vinatier et al., 2015) are either not present or not readily

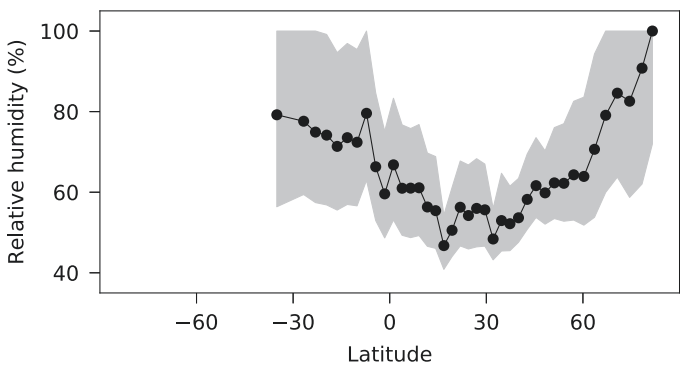

Fig. 3

Estimated latitudinal variations of near-surface relative humidity for late northern spring, from ground-based near-infrared observations and *Cassini* surface brightness temperature measurements. Shading shows uncertainty. *Adapted from Lora, J.M., Ádámkovics, M. 2017. The near-surface methane humidity on Titan. Icarus, 286, 270–279.*

observable in the lower atmosphere. Similarly, atmospheric features like clouds, in addition to being sparse, are prone to modification by waves (see Section 2.3), so they are not always reliable indicators of the background winds. As a result, the only unambiguous estimates of wind speeds come from in situ measurements.

The *Huygens* probe's descent provided such measurements: Fig. 2 shows the zonal winds from ground-based Doppler measurements of the *Huygens* radio signal (Bird et al., 2005) and the meridional winds inferred from the motion of the probe (Karkoschka, 2016) for the lowermost 20km. Intriguingly, both profiles show changes in wind direction at the same altitudes: Nearest the surface, the wind experienced by *Huygens* was clearly southeastward, with a magnitude peaking at about $1\,m\,s^{-1}$; at pressures lower than roughly 1400hPa (altitudes above 1km), the wind blew westward and somewhat northward; finally, at about 1100hPa (roughly 6km), the meridional component essentially vanished and the wind was again eastward. Encouragingly, GCMs seem to reproduce this near-surface wind structure for the latitude and season of the *Huygens* measurements (Lora et al., 2019), suggesting that it is dominantly set by the large-scale circulation, which is captured by such simulations.

An additional curiosity is that the region of roughly constant specific humidity measured by *Huygens* also coincided with the altitudes of reversing winds (Fig. 2). Especially since this constant value implies mixing, these observations seem to suggest a shallow but vigorous overturning circulation (see Charnay and Lebonnois, 2012)—presumably a cross-equatorial Hadley cell with rising air in the southern (summer) hemisphere and descending motion in the northern (winter) hemisphere, and thus northward flow aloft and southward return flow near the surface at 10°S. That this inferred circulation is shallow and primarily confined to the lowest 6 km of the atmosphere lends further credence to the idea that the lower latitudes are dry, based on expectations from GCMs (Mitchell, 2008). Therefore, this is additional evidence of the importance of the large-scale circulation in setting the humidity of Titan's equatorial region.

Finally, we can estimate, for the *Huygens* site, the meridional transport of methane moisture by the atmosphere, which is simply the mass-weighted product of the meridional wind and specific humidity at each level of the atmosphere. The result is shown in the right panel of Fig. 2. Unsurprisingly, this too shows two general regions associated with the overturning circulation: a strong southward transport along the surface, and a northward transport between 1400 and 1100hPa (1–6km). If we assume that this is indeed representative of the Hadley circulation throughout the low latitudes, these measurements are evidence of cross-equatorial moisture transport. Interestingly, the vertical integral of the estimated transport yields a modest positive value—that is, a net export of moisture from the southern hemisphere northward in the southern mid-summer. But, of course, this isolated estimate provides no information on the full seasonal cycle of atmospheric moisture transport, its annual behavior, or its variability.

2.2 Observations of clouds and rain

Titan's clouds have been documented since 1995 with Earth-based telescopes, including the Hubble Space Telescope, the United Kingdom Infrared Telescope, Gemini, and Keck Observatories (Griffith et al., 1998; Roe et al., 2002; Lemmon et al., 2019; Corlies et al., 2019). During the *Cassini* mission from 2004 to 2017, the on-board Imaging Science Subsystem (ISS; Porco et al., 2004) and Visual and Infrared Mapping Spectrometer (VIMS; Brown et al., 2004) monitored Titan's cloud activity (Rodriguez et al., 2011; Turtle et al., 2018), along with Earth-based observation campaigns (Schaller et al., 2006a,b, 2009). These observations provide important information about cloud structure and morphology, short-term behavior (on timescales of hours to days), and longer term seasonal patterns. In particular, the high spatial and temporal resolution of *Cassini* observations, with imaging typically every 1–2 Titan days especially during the later part of science operations, documented cloud locations over almost half a Titan year, from late southern summer through the northern summer solstice; over this time, cloud activity was generally observed to follow the seasonal insolation (Fig. 4), although lagging seasonal changes due to the atmosphere's high inertia (Turtle et al., 2011a, 2018).

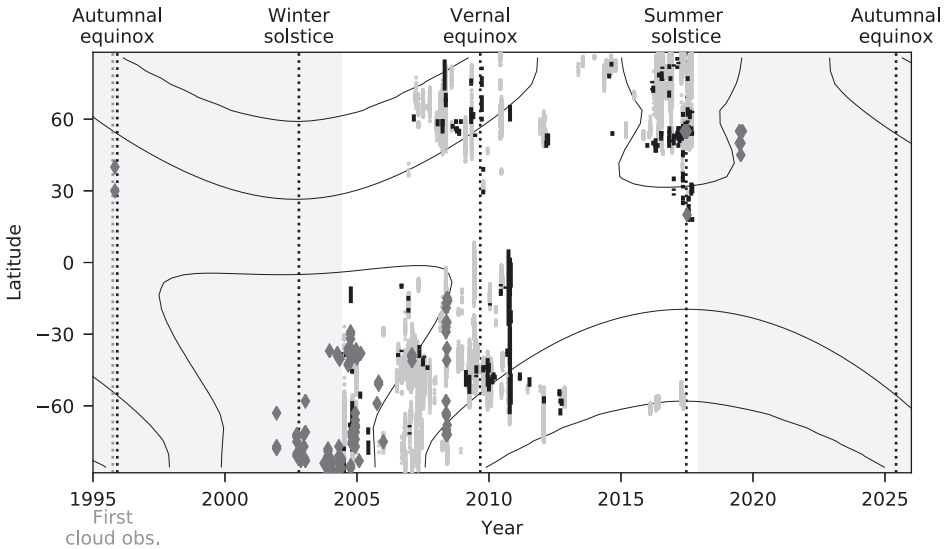

Fig. 4

Latitudinal distribution of observed lower atmospheric clouds through about one Titan year. Observations from *Cassini* ISS (*black*) and VIMS (*gray*) (Turtle et al., 2018; Rodriguez et al., 2018), and various ground-based studies (*dark gray diamonds*; Brown et al., 2002; Roe et al., 2002; Bouchez and Brown, 2005; Roe et al., 2005; Schaller et al., 2006a, 2009; Ádámkovics et al., 2010; Lemmon et al., 2019; Corlies et al., 2022) are shown. The distribution of diurnal average insolation at the top of the atmosphere is shown for reference (*thin black curves*). Times of the first cloud detection (Griffith et al., 1998), northern autumnal and vernal equinoxes, and winter and summer solstices are shown by *dashed vertical lines*. Times before and after the *Cassini* mission are shaded *light gray*.

A variety of cloud types and spatial scales have been observed (Fig. 5). Morphological categories and the extent of clouds observed by *Cassini* ISS and VIMS are documented in Turtle et al. (2018). From Earth-based telescopes, only larger events (scales on the order of hundreds of km) can be observed, with an observational bias toward subsolar latitudes; *Cassini* provided observations of clouds at a range of scales down to a few kilometers. During late southern summer (2004–2005), *Cassini* detected fields of clouds exhibiting convective

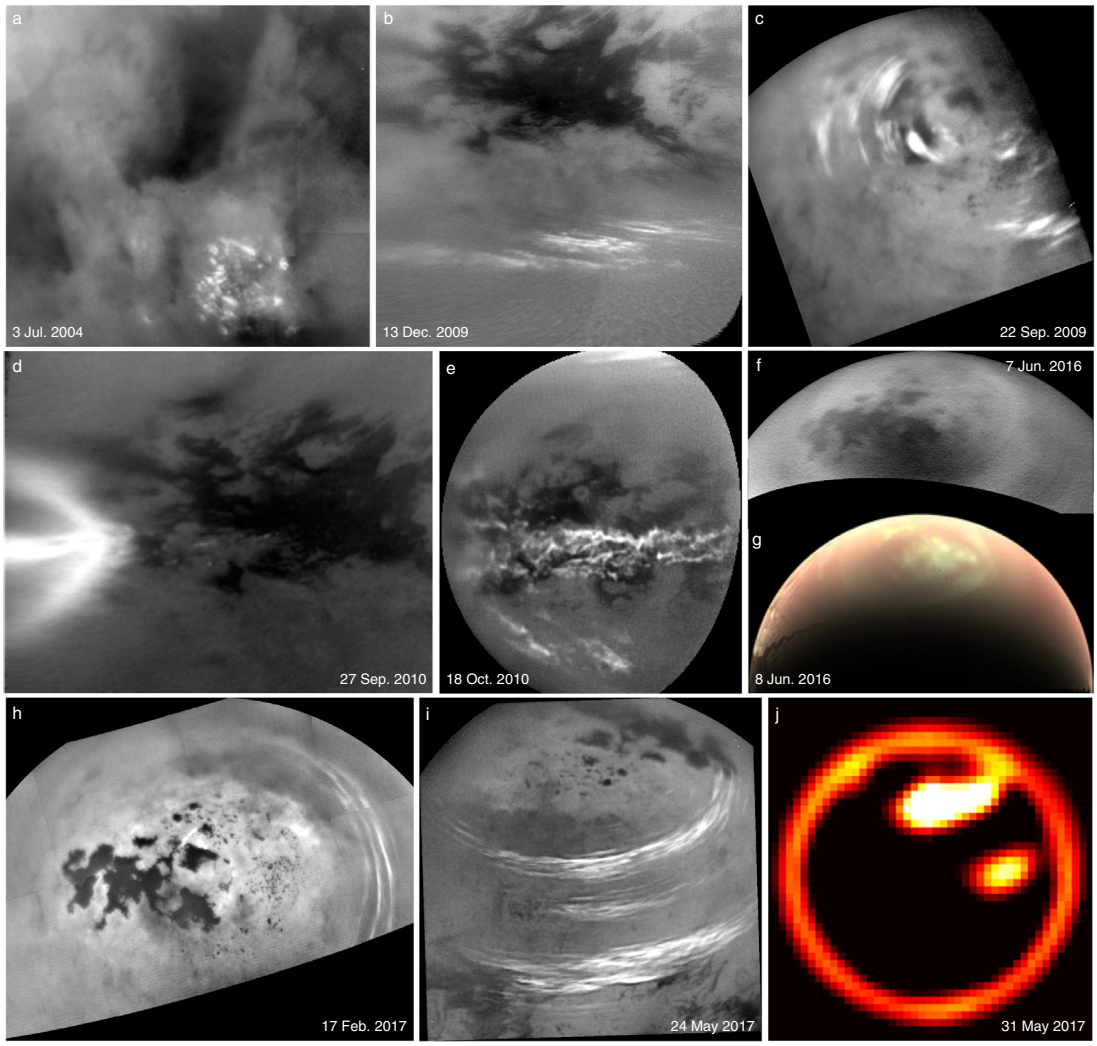

Fig. 5

Observed clouds in Titan's lower atmosphere. Examples of observations from *Cassini* ISS (A–F, H, I), VIMS (G), and ground-based facilities (J) (Gemini NIRI; Corlies et al., 2022), showing the diversity of methane clouds on Titan. Dates of observation are shown in each panel.

behavior above the south pole (Porco et al., 2005; Turtle et al., 2009) (Fig. 5A). Isolated small clouds were observed infrequently at lower latitudes, where in some cases VIMS spectral observations provided confirmation of short-term altitude evolution consistent with convective cells (Griffith et al., 2005). As the subsolar point moved northward, elongated cloud streaks became common at mid-southern latitudes, especially from late 2006 to 2010 (Fig. 5B). These clouds were initially consistent with atmospheric models; however, clouds continued to form in these locations for substantially longer than initially predicted (Turtle et al., 2009). Over a similar time period, methane clouds also formed at high northern latitudes (Fig. 5C); these were frequently observed from 2007 to 2010. In Titan's late northern spring, elongated streak clouds became common at mid-northern latitudes, and smaller, isolated cells were observed near the north pole (Fig. 5H and I).

The onset of summer clouds at high northern latitudes was long anticipated (and led to some of the questions that remain outstanding after *Cassini*; Nixon et al., 2018). As Titan's northern spring progressed, monitoring continued with the ISS and VIMS instruments, but substantial north polar cloud activity lagged predictions that large events might occur as early as 2010. North polar cloud activity did not become common until around 2016 (Fig. 4) and generally consisted of smaller isolated clouds rather than the large systems that had been expected based on observations of high southern latitudes during late southern summer, though Earth-based observations detected large northern events near the end of the *Cassini* mission and afterward (Fig. 5J; Corlies et al., 2022). Another surprise was that, in some cases, apparent cloud detections by VIMS (Fig. 5G) coincided with ISS observations of Titan's surface that were unobstructed by clouds (Fig. 5F). The appearance of clouds to VIMS at 2.1 and 2.75μm but not to ISS at 0.94μm is not yet understood, although one hypothesis is that these clouds could have represented high-altitude cirrus or consisted of very small droplets that were optically thick compared to Titan's atmospheric haze at longer wavelengths but optically thin compared to the haze at shorter wavelengths (Turtle et al., 2018).

In addition to these relatively common cloud types, there have been some suggestions of possible associations with surface features. For example, some observations could be consistent with the formation of lake-effect clouds (e.g., Brown et al., 2009a; Turtle et al., 2011a); however, data limitations prevent these interpretations from being definitive, and cloud-resolving models have not convincingly produced such features associated with air–sea interactions (Chatain et al., 2024; Rafkin and Soto, 2020). Similarly, distinguishing low-altitude clouds from true ground fog has proven difficult (Brown et al., 2009b; Smith et al., 2016; Rafkin and Soto, 2020; Dhingra et al., 2020).

In a few instances, *Cassini* also observed evidence of rainfall, consisting of changes detected on Titan's surface coincident with cloud detections. Following a large cloud outburst at the south pole in late 2004 (Schaller et al., 2006a; Turtle et al., 2011c) and another at about 30°S in 2010 (Turtle et al., 2011a), large areas of the surface darkened; these were interpreted to be the result

of wetting by methane rainfall (Turtle et al., 2009, 2011b). The south-polar event darkened an area of more than 30,000 km^2, and the one observed at lower latitudes affected an area of roughly 500,000 km^2. Some locations also subsequently brightened, potentially as a result of frost deposition from local cooling of the surface due to evaporation (Barnes et al., 2013). Following both of these events, the surface returned to its prerainfall appearance over a timescale of several months. An additional interesting implication of these events for Titan's weather is that each seems to have been followed by a period of suppressed cloud activity (Fig. 4) (e.g., Schaller et al., 2006b).

Finally, the surface transiently brightened near the north pole following the VIMS detection of clouds at longer wavelengths in 2016 (see above); Dhingra et al. (2019) hypothesized that this brightening was due to specular reflection from a wet solid surface covering an area of about 120,000 km^2. In this case, there was no concomitant surface darkening detected by ISS, so, as with the unusual spectral properties of these north-polar cloud features, questions remain regarding these effects and their implications for Titan's weather and interactions with the surface.

2.3 Mechanisms of cloud formation

The presence of discrete, quickly evolving clouds correlated with seasonal surface forcing implies that moist convection is an important mechanism on Titan. Convection mixes air vertically, altering the environmental temperature and humidity structure: Deep convection consumes convective available potential energy and converts it to kinetic energy, at the same time releasing latent heat and potentially humidifying upper levels (e.g., Rafkin et al., 2022). Cloud-resolving simulations of Titan demonstrate that, when deep convection occurs, copious precipitation can result (Hueso and Sánchez-Lavega, 2006; Barth and Rafkin, 2007, 2010; Rafkin and Barth, 2015). However, the same models demonstrate that Titan's environment as measured by *Huygens* was not conducive to convection (Barth and Rafkin, 2007); deep convection can only occur with considerably more humid lower levels (Barth and Rafkin, 2007, 2010; Griffith et al., 2008; Rafkin et al., 2022). In addition, the availability of convective available potential energy is insufficient to predict convection; if moist near-surface air parcels must be lifted through drier regions before reaching saturation, lateral mixing can dilute their buoyancy (Rafkin et al., 2022). As a result, shallow, nonprecipitating convection may be relatively common on Titan (as on Earth), while large storms require particular conditions that could depend on organization by the large-scale circulation.

As described in Section 2.1, Titan's atmospheric environment around 5–20 km is observed to have roughly uniform temperature and very little seasonal variation. On theoretical grounds, this arrangement is to be expected since the confining influence of the Coriolis effect on horizontal heat transport is weak, as in Earth's tropics, because of Titan's slow rotation. Horizontally propagating gravity waves travel efficiently along the atmosphere's stable stratification, preventing strong temperature gradients from developing; this is the so-called

weak temperature gradient (WTG) dynamical state (Sobel et al., 2001). In the WTG regime, local near-surface enhancements of moist static energy—a measure of the total internal, potential, and latent energy of the local air—are the preferred locations for deep convection (see Schneider et al., 2012; Mitchell and Lora, 2016). Parsing these into energy components, this is equivalent to saying that convection and clouds should be expected to form above enhancements in temperature and/or humidity of the near-surface atmosphere. There are at least three ways this can occur: evaporation of surface liquids; surface temperatures that follow the seasonally evolving subsolar latitude, modulated by various surface inhomogeneities; and convergence of moisture by the atmospheric circulation. We next focus on this latter possibility, mainly associated with waves: In the WTG regime, any type of circulation that converges moisture in the near-surface environment has the potential to produce deep, precipitating convection.

Atmospheric waves can be categorized as tropical and extratropical. Gravity waves—those wherein the restoring force is buoyancy—naturally produce ascending and descending motion with convergence and divergence between. At the planetary scale, various waves can be expected to play an important role in organizing clouds and convection. The Kelvin wave, a type of gravity wave that propagates eastward along the equator (Matsuno, 1966; Kiladis et al., 2009), can extend widely in latitude on Titan and therefore exert a broad influence. Indeed, a Kelvin wave was the likely cause of the observed large-scale cloud outburst that occurred just following the vernal equinox in 2009 (Fig. 5D), which appeared as an eastward-pointing arrow centered on the equator (Turtle et al., 2011a): GCM simulations demonstrated that, at the same season as this event, Kelvin waves are active and organize storms into eastward-pointing chevrons similar in shape to the observed cloud (Fig. 6) (Mitchell et al., 2011).

Within a few weeks of the arrow cloud, a second cloud outburst was observed, this time with a band stretched along the equator and a streak extending eastward and away from the equator (Fig. 5E). Again, GCM simulations produced this type of morphology at the same season, suggesting the underlying mechanism to be an extratropical Rossby wave interacting with the tropical circulation (Mitchell et al., 2011). Geophysically pure Rossby waves—waves associated with the latitudinal variation in the Coriolis force, which propagate westward relative to the background flow—do not produce convergence, but they cause neighboring air masses to interact strongly when aided by boundary layer friction in a process called frontogenesis (e.g., Hoskins, 1982). The streak cloud was likely the result of surface-level convergence by such frontogenesis, very much like the cold front clouds and precipitation experienced in Earth's mid-latitudes. Interestingly, some time earlier (just prior to Titan's vernal equinox), ground-based observations indicated a pulse of low-latitude clouds followed by activity at southern latitudes, similarly related to the propagation of Rossby waves (Schaller et al., 2009). Thus, it appears that two pulses of springtime clouds occurred during the *Cassini* years; that both were associated with atmospheric waves suggests these, along with seasonably favorable conditions for convection, are crucial for cloud formation.

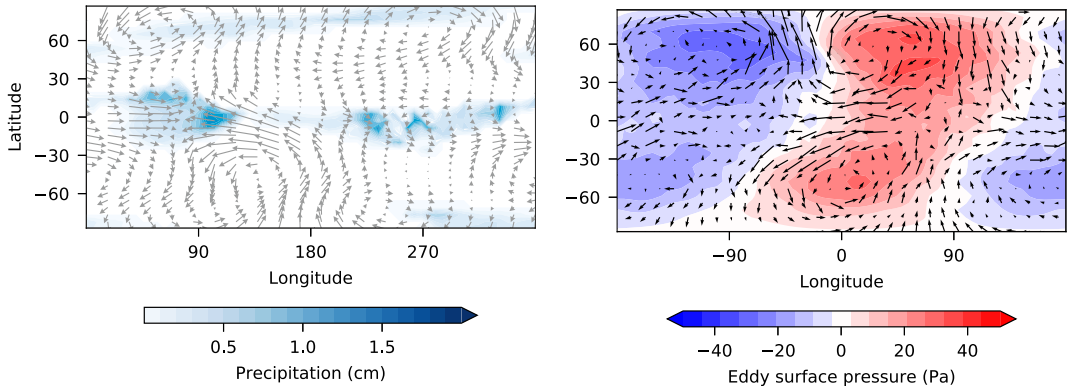

Fig. 6

Atmospheric waves in simulations of Titan. *Left*: Precipitation (*colors*) and eddy near-surface winds (*arrows*) caused by a Kelvin wave-like disturbance during the equinoctial season simulated in a GCM; compare to Fig. 5D. *Right*: Eddy surface pressure (*colors*) and eddy near-surface winds (*arrows*) showing waves excited globally by solstitial polar convection, as simulated by another GCM. *Adapted from Mitchell, J.L., Ádámkovics, M., Caballero, R., Turtle, E.P. 2011. Locally enhanced precipitation organized by planetary-scale waves on Titan. Nat. Geosci. 4, 589–592 and Battalio, J.M., Lora, J.M. 2021b. Global impacts from high-latitude storms on Titan. Geophys. Res. Lett., 48, e2021GL094244.*

In fact, Rossby waves and frontogenesis are predicted to be common throughout Titan's high latitudes, and these too are associated with seasonal storms (Lora and Mitchell, 2015; Battalio and Lora, 2021b). Recent GCM simulations showed that extratropical Rossby waves are ubiquitous at high latitudes; during summertime, the phase of such waves can coincide with sufficient thermodynamic instability locally to generate a pulse of deep convection (Battalio and Lora, 2021b). In the simulations, this interaction temporarily halts the wave propagation—a prediction of stationary clouds; indeed, several observations of clouds have suggested seemingly stationary cloud systems (Roe et al., 2005; Schaller et al., 2006a; Ádámkovics et al., 2010). Interestingly, the convection then forces additional waves—including equatorial Rossby and mixed Rossby-gravity waves (Fig. 6)—that communicate the disturbances globally (Battalio and Lora, 2021b). One implication of this is that strong polar storms on Titan might have even equatorial consequences. More broadly, all of these findings indicate that clouds on Titan are intimately connected to waves. This in turn suggests that cloud activity may also be linked to other types of as-yet-undiagnosed atmospheric waves. Furthermore, it illustrates that disentangling clouds from waves is difficult, since the evolution of clouds may be more closely related to wave propagation than to the background flow.

Of course, any region of the atmosphere that becomes saturated with methane vapor will condense and form clouds of liquid and/or ice, so long as there is an energy sink to remove the latent heat. This need not involve deep convection, nor waves (though it could equally be associated with waves of all sorts). A good example of this is the winter polar cap cloud

observed at around 40km altitude as Titan's north pole emerged from the polar night (Griffith et al., 2006). Without sunlight, the atmosphere passively cools to space, which offsets the latent heat release in the cloud. Once sunlight returns in spring, the cloud dissipates as temperatures rise. It is thought that the north polar cap cloud was composed primarily of ethane rather than methane, but the physical mechanism of its formation is the same (Griffith et al., 2006). Other cloud formation mechanisms are also possible; some examples include frontal lifting of a moist boundary layer, orographic waves, and convergence of heat and/or moisture by tropospheric waves outside of the boundary layer.

3 Titan's climate and its variability

Having discussed observations and simulations of weather phenomena, we next turn to Titan's large-scale atmospheric circulation and climate. The general circulation refers to the combination of macroscopic motions creating and sustaining time-mean winds, temperature, and other atmospheric fields. On Earth, the tropical circulation is qualitatively distinct from the extratropical circulation, the former being dominated by a zonally symmetric overturning called the Hadley circulation and the latter by zonal jet streams interacting with storm tracks. Not coincidentally, the latitudinal extent of the Hadley cells roughly corresponds to the WTG regime, and due to the considerations mentioned earlier, the surface-level convergence of the Hadley circulation—the intertropical convergence zone (ITCZ)—dominantly contributes to deep convection and cloud formation. Titan's general circulation differs from Earth's in two very important ways. First, due to Titan's slower rotation and smaller size, its Hadley cells span a wider swath of latitudes (e.g., Mitchell et al., 2006) (Fig. 7). The overturning is also seemingly layered, somewhat obfuscating the depth of the planetary boundary layer (Charnay and Lebonnois, 2012). Second, Titan's ITCZ follows the solar forcing deep into the summer hemisphere. From this combination of effects, there are preferred latitudes of cloud formation that evolve seasonally (Figs. 4 and 7); this is borne out in GCM simulations (Mitchell et al., 2006; Rannou et al., 2006; Mitchell, 2008; Schneider et al., 2012; Lora et al., 2015, 2022; Newman et al., 2016; Faulk et al., 2020). Titan's extratropics—latitudes poleward of the Hadley circulation—correspondingly span a narrower range of latitudes than on Earth. Perhaps less obviously, the extratropical storm tracks are also weaker on Titan due to weak temperature gradients in latitude; there is less potential energy available to drive them (Lebonnois et al., 2012; Lora and Mitchell, 2015; Mitchell and Lora, 2016). The disturbances that make up the storm tracks are also shallow because, rather than being constrained by the vertical scale height, the instabilities that drive them occur at the largest horizontal scales (Lora and Mitchell, 2015; Mitchell and Lora, 2016).

At the scale of the climate, Titan's slow rotation, cold and massive atmosphere, and surface properties dictate the large-scale features of the circulation, captured to first order by the dominant force balances and relevant timescales. First, as in nearly all planetary atmospheres,

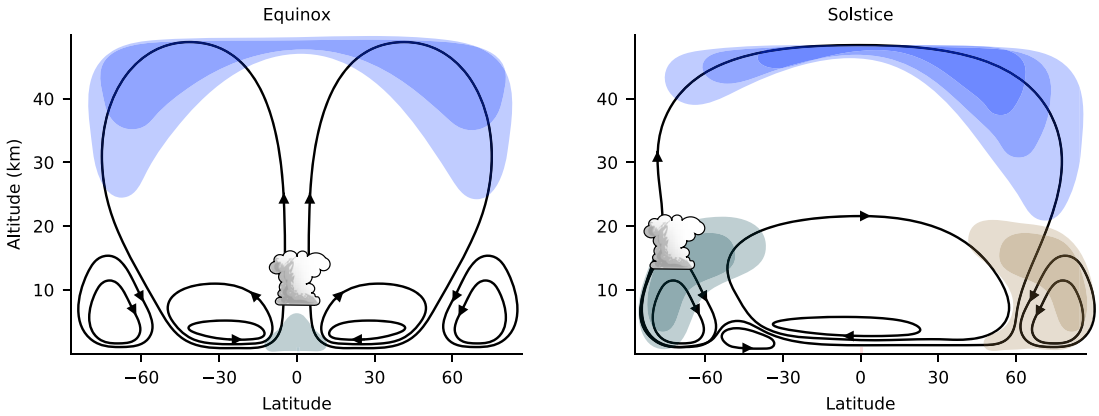

Fig. 7

Schematic illustration of the circulation in Titan's lower atmosphere during equinox (*left*) and southern summer solstice (*right*). Curves with arrows depict the meridional mass stream function; the cells that extend to higher altitudes comprise the Hadley circulation, while the shallow high-latitude ones are Titan's extratropical cells. *Blue* contours near the top illustrate westerly winds roughly 10 m s^{-1} and stronger (deeper color represents higher magnitude), and their relationship to the overturning circulation. Colors near the surface indicate regions of anomalously high (*blue-green*) and low (*brown*) specific humidity relative to the annual average. Clouds show preferred latitudes for precipitation.

the hydrostatic balance between the vertical pressure gradient force and gravity is a very good approximation on Titan (Mitchell and Lora, 2016). Horizontal force balance is divided into vertical regions based on the local value of the Rossby number, which is a measure of the relative magnitudes of inertial and Coriolis forces. The Rossby number is large in Titan's superrotating stratosphere, and the dominant force balance is therefore cyclostrophic—a balance between pressure gradient and centrifugal forces (e.g., Flasar et al., 1981; Flasar and Achterberg, 2009). In the lower atmosphere, winds are weak, the Rossby number is smaller, and the balance is geostrophic; that is, between horizontal pressure gradient and Coriolis forces (Bird et al., 2005; Mitchell and Lora, 2016). An intermediate region in gradient wind balance—a three-way force balance between pressure gradient, centrifugal, and Coriolis forces—connects the upper cyclostrophic and the lower geostrophic layers.

A number of timescales related to Titan's climate can be estimated (e.g., Mitchell and Lora, 2016). The seasonal timescale, set by Saturn's orbital period of 29.5 Earth years, and lethargic radiative relaxation (longer than a Titan year) have already been mentioned (Section 2.1). Closely related, the dynamical overturning time of the circulation is similarly long (Mitchell and Lora, 2016). Though the atmospheric temperature response to cyclical seasonal forcing lags the forcing by a quarter cycle (Flasar et al., 1981; Mitchell et al., 2006), a strong seasonal cycle can be present in Titan's troposphere because the surface and boundary layer have a low thermal inertia: Qualitatively, the surface and boundary layer are subjected to a radiative imbalance as the pattern of insolation shifts with seasons. In the spring, the surface warms faster

than the overlying atmosphere, communicates this warming to the lower atmosphere through boundary layer energy fluxes of sensible and latent heat, and creates static instability that drives convection through a depth in the atmosphere dependent on the buoyancy flux at the surface (Mitchell and Lora, 2016). In this way, the depth of convection determines how much the long radiative timescales dampen the seasonal cycle.

Three other timescales related to the methane cycle are also important to consider. First is the residence time of methane in the atmosphere, which, based on local considerations of the global surface energy budget, is of the order of the orbital period (Mitchell, 2012); this is consistent with episodic storms throughout the seasonal cycle. The second is the timescale of infiltration of methane into Titan's surface regolith. This is highly uncertain, but a reasonable estimate puts it at about the orbital period as well (Hayes et al., 2008). The third is that of orbital precession, which is about three orders of magnitude larger than the orbital period and might influence the transfer of methane from one hemisphere to the other. The processes associated with all of these timescales are further discussed in the following sections.

3.1 Influence of the surface

It has become increasingly obvious that Titan's surface exerts an important influence on its climate. Pre-*Cassini* expectations of a lack of seasonality based on the huge thermal inertia of Titan's massive atmosphere (e.g., Flasar et al., 1981) did not bear out, and, as described in Section 2.1, observations of the surface temperature clearly show seasonal changes consistent with a low thermal inertia—a situation rather different than on Earth, where the oceans' high inertia buffers seasonal variations. In fact, some of the first observed south polar clouds on Titan were interpreted as indicating a maximum surface temperature at the pole, given the high obliquity (Brown et al., 2002). The situation is more complicated, since even at solstice the insolation reaching the surface peaks at mid-latitudes and not the pole as a result of the atmospheric opacity (Lora et al., 2011); nevertheless, a low thermal inertia is a prerequisite for strong seasonal variations.

The thermal properties of the surface have been of interest for some time, including after a $\sim$3K equator-to-pole temperature gradient was inferred from *Voyager* data (Samuelson et al., 1997; Courtin and Kim, 2002). Tokano (2005) investigated the effects of three different, but in each case globally homogeneous, surface types in a dry GCM (that is, a model excluding the effects of phase changes of methane) and found that these temperature gradients were best recovered in the simulation with the lowest thermal inertia ($335\,\mathrm{J\,m^{-2}\,s^{-\frac{1}{2}}\,K^{-1}}$), corresponding to a surface made up of a "porous icy regolith." In addition, this simulation produced superadiabatic near-surface layers that coincided with the location of observed clouds at the time (the model did not include a convective parameterization), but also summer-to-winter swings of 3–4K at the poles that are too large (see Fig. 1). With a different model, Lebonnois et al. (2012) examined the difference between using a relatively high surface thermal inertia and one similar

to the icy regolith case, and (predictably) found that the latter produced seasonal temperature variations of larger magnitude with maxima that extended farther poleward in summer. Finally, MacKenzie et al. (2019) generated a global map of thermal inertia based on terrain types mapped from *Cassini* data and implemented it in a third GCM. Presumably because the thermal inertia estimated for the different terrains covered a relatively limited range of one order of magnitude (from a low in the equatorial dunes to a high in the hummocky regions), the effects of heterogeneous thermal inertia had only a minimal influence compared to the case employing a globally averaged value of $750\,\mathrm{J\,m^{-2}\,s^{-\frac{1}{2}}\,K^{-1}}$. This suggests that future models can use this single value—modestly larger than the original "porous icy regolith"—to investigate Titan's climate at all but the finest scales.

Importantly, all of the aforementioned simulations used model configurations neglecting the methane cycle. In the case of MacKenzie et al. (2019), this was done specifically to isolate the influences of the surface thermal inertia, as previous results with the same model demonstrated the importance of latent heat fluxes to the simulated distribution of surface temperatures (Lora et al., 2015; Lora and Ádámkovics, 2017); this is consistent with many other studies (e.g., Mitchell, 2008; Newman et al., 2016; Tokano, 2019; Faulk et al., 2020). Indeed, the possibility of surface evaporation controlling surface temperatures was recognized even in the context of the *Voyager* results: Stevenson and Potter (1986) suggested that polar temperatures on Titan might be determined by the dew point of methane–nitrogen lakes and therefore effectively constant, even before such lakes were discovered. (Of course, this does not occur either, as polar temperatures do vary seasonally.)

Considering the distribution of methane in Titan's climate system, two end-member states seem to be possible for modern Titan: one with ample surface liquid, and one where the vast majority of the methane directly accessible to the atmosphere exists in the vapor phase (and the surface is therefore quite dry) (Mitchell, 2008). In the former case, the latitudinal surface temperature distribution is lower and flatter (Mitchell, 2008; Lora et al., 2015), and inconsistent with observations (Lora and Ádámkovics, 2017). The latter drier case also better reproduces the vertical profile of methane at the equator, as observed by *Huygens*, enabling a region of near-constant methane mole fraction in the lowest few kilometers of the atmosphere that does not form in the presence of global surface liquids (Mitchell, 2008; Lora et al., 2015; Lora and Ádámkovics, 2017). Lastly, the seasonal distribution of precipitation predicted by GCMs under these two regimes is entirely different: With (quasi-) global surface liquids, a band of effectively continuous precipitation oscillates seasonally between hemispheres; in the drier case, this band is largely absent, and summer polar precipitation dominates, with sporadic activity elsewhere (Mitchell et al., 2006; Mitchell, 2008; Schneider et al., 2012; Lora et al., 2015; Mitchell and Lora, 2016; Newman et al., 2016; Turtle et al., 2018). While neither of these provides a great match for observed clouds (see Fig. 4), the former is decidedly inconsistent with observations (Turtle et al., 2018), again suggesting that Titan's climate is mostly dry.

Obviously, there is neither an ocean of methane nor an entirely dry surface on Titan. In addition to the lakes and seas observed by *Cassini* (Stofan et al., 2007; Stephan et al., 2010), which clearly cluster at polar latitudes (Aharonson et al., 2009; Hayes, 2016), there is also widespread evidence of flowing liquid (present or past) across the surface (e.g., Langhans et al., 2012; Burr et al., 2013; Birch et al., 2016; Poggiali et al., 2016), including in the arid equatorial landscape on which *Huygens* landed (Tomasko et al., 2005), suggesting pluvial activity globally. Yet the lake districts, in particular, may be of outsized importance: Despite the fact that the vast majority of the methane inventory observed by *Cassini* exists in the atmosphere (Tokano et al., 2006; Lorenz et al., 2008a) and that the volume of the observed lakes is insufficient to replenish losses from the atmosphere, recent observations indicate that the lower atmospheric humidity varies substantially with latitude (Section 2.1; Ádámkovics et al., 2016; Lora and Ádámkovics, 2017). Indeed, Lora and Ádámkovics (2017) suggested that the near-surface relative humidity varies by close to a factor of two between low and high latitudes, from roughly 50% near the equator to up to 100% over the poles (Fig. 3), consistent with GCM simulations in which the entire polar surfaces are a source of methane.

Furthermore, numerous indications exist that Titan's charismatic seas are not the sole reservoir of liquid methane in the polar regions. First, the northern seas seem to share an equipotential surface, as do many of the lakes within individual drainage basins, implying the existence of a subsurface methane table that connects these surface expressions (Hayes, 2016; Horvath et al., 2016; Birch et al., 2017; Hayes et al., 2017). Second, surface brightness temperatures over the north pole, even in land areas outside of the seas, warmed more slowly during spring than would otherwise have been expected from dry ground, suggesting evaporative cooling of moist ground (Jennings et al., 2016). Third, Titan shows a paucity of impact craters, but those that exist tend to occur at lower latitudes and higher-than-average elevations, indicating that impacts at lower elevations may have interacted with a methane table, leaving scant surface manifestations (Neish and Lorenz, 2014). Finally, GCM simulations indicate that evaporation from only the surfaces of observed seas and lakes is insufficient to support an active hydroclimate (Tokano, 2009; Lora et al., 2015), leading to a throttled hydrologic cycle that contradicts observations—Titan has an arid climate, but it is not completely desiccated.

Instead, models wherein substantial portions of the polar surfaces are wet and able to evaporate—consistent with the aforementioned evidence for a widespread methane table—reproduce many of the observed characteristics listed earlier, most notably the distributions of temperatures, tropospheric humidity, and seasonal precipitation (a proxy for clouds) (Lora and Mitchell, 2015; Mitchell and Lora, 2016; Lora and Ádámkovics, 2017; Lora et al., 2019). The polar surfaces humidify the overlying boundary layer, allowing for deep convection that humidifies the troposphere, and this atmospheric humidity is transported to other latitudes by the general circulation (Fig. 7), via eddies and the meridional Hadley circulation (Mitchell, 2012; Lora and Mitchell, 2015; Mitchell and Lora, 2016; Lora and Ádámkovics, 2017; Battalio and Lora, 2021b; Battalio et al., 2022).

Crucially, a recent model that synchronously coupled the atmospheric circulation to active land hydrology self-consistently reproduced the presence of near-surface methane liquid in the polar regions (Faulk et al., 2020). In this model, large-scale surface runoff and liquid flow through porous regolith depend on Titan's topography, using estimates from *Cassini* (Corlies et al., 2017). Because the polar regions are depressed, compared to lower latitudes, relative to an equipotential surface (Lorenz et al., 2013; Mitri et al., 2014; Corlies et al., 2017), runoff tends to route precipitated methane poleward and, additionally, the top of a methane table is much closer to the surface near the poles. Consequently, the results of Faulk et al. (2020) qualitatively reproduce the distribution of Titan's seas and lakes and, at the same time, predict the presence of near-surface ground methane throughout the polar regions that allows evaporation into the atmosphere. As in other GCMs that impose polar methane, this model simulates seasonal precipitation patterns with ample summer polar precipitation; occasional precipitation at lower latitudes, fed by atmospheric moisture transport, produces surface liquid that largely runs off or infiltrates into the subsurface, such that the equatorial regions remain deserts, as observed (Fig. 8).

Other aspects of Titan's surface may also affect its atmosphere and climate. Variations in the emissivity of Titan's surface (Janssen et al., 2016) and the albedo could affect the surface energy balance, though these appear to be secondary considerations for the climate (Tokano, 2019), as are regional variations of the thermal inertia (MacKenzie et al., 2019). Interestingly, the direct topographic forcing of the atmospheric circulation—separate from its importance for

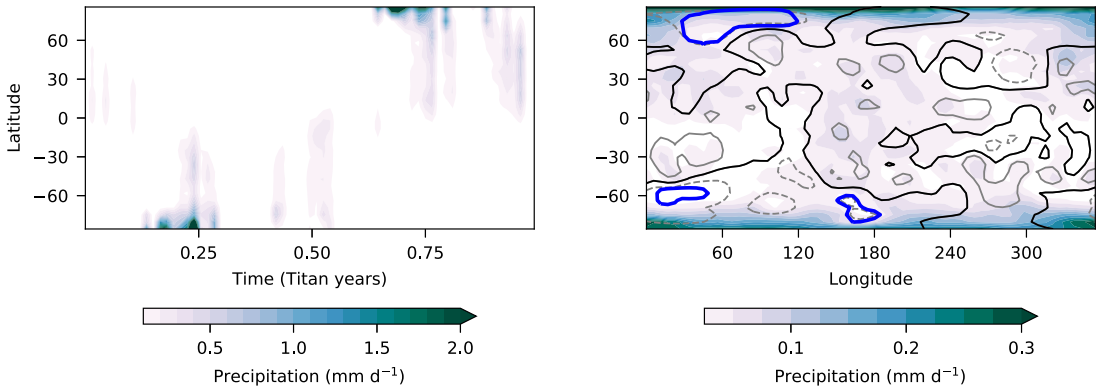

Fig. 8

Simulated precipitation. *Left*: Seasonal evolution of longitudinally averaged precipitation from 10 years of simulation with a GCM (Lora et al., 2022). *Right*: Map of annually averaged precipitation from the same simulation (filled contours), overlain with the relative topography used in the model (from Corlies et al., 2017) (*black contour* shows average topography; *gray solid* and *dashed contours* show higher and lower topography, respectively, with 300m interval), and the locations of simulated surface liquids (*blue contours*). *Adapted from Lora, J.M., Battalio, J.M., Yap, M., Baciocco, C. 2022. Topographic and orbital forcing of Titan's hydroclimate. Icarus, 384, 115095.*

land hydrology—may be important. Despite the low surface relief (the tallest mountain peaks may be a few km; Radebaugh et al., 2007) relative to the atmospheric scale height (roughly 20 km), Titan's static stability (Brunt–Väisälä frequency $\sim 0.002\,s^{-1}$) and modest near-surface wind speeds ($1–2\,m\,s^{-1}$; see Fig. 2) suggest that even 1 km relief is sufficient to split the flow (see, for example, Smith, 2019). On the other hand, upslope flow—particularly over mountain ridges that prevent flow splitting—can lead to sufficient vertical motion to initiate cloud formation, under certain circumstances potentially even enabling deep convection (Barth, 2010). Even in dry GCM simulations, elevated topography produces near-surface convergence (which is associated with rising motion); conversely, local depressions lead to divergence (Tokano, 2008). Indeed, recent simulations, including the methane cycle, incorporating the topography map estimated from *Cassini* data (Corlies et al., 2017) produce generally enhanced (suppressed) precipitation over topographic highs (lows) relative to simulations with a flat surface (Lora et al., 2022). As a consequence, mid-latitude precipitation is more common in simulations with topography (Fig. 8). At the same time, topography also causes the polar regions, which are relatively low-lying, to have elevated surface temperatures as a result of the atmospheric lapse rate; this in turn can enhance evaporation from the surface and subsurface methane reservoirs (Lora et al., 2022).

3.2 Influence on the surface

Of course, the influences between the surface and atmosphere go in both directions. While properties of the surface enable the relatively strong seasonality of the circulation and methane cycle of the lower atmosphere, these in turn strongly affect the surface itself. In this sense, the average climate is important—the poles are humid; the equator is dry—but in addition variability exerts a key influence: Much evidence exists of rain- and wind-driven erosion (e.g., Tomasko et al., 2005; Lorenz et al., 2006, 2008b; Perron et al., 2006; Jaumann et al., 2008; Radebaugh et al., 2008; Langhans et al., 2012; Burr et al., 2013; Birch et al., 2016; Neish et al., 2016; Hedgepeth et al., 2020), both of which depend strongly on the magnitude of these phenomena and therefore on their extrema. Additionally, GCM simulations show that year-to-year variability is significant, particularly in precipitation (Faulk et al., 2017; Lora et al., 2019), and further suggest that Titan may support some large-scale patterns of variability that are reminiscent of Earth's (Battalio and Lora, 2021a). All of these point to the importance of Titan's climate variability, both spatial and temporal.

Prior to *Cassini*, erosion by rain was predicted to be minimal (Lorenz and Lunine, 1996) based on the slow terminal speed of raindrops (Lorenz, 1993), though subsequent work showed that large drops could reach the surface (Graves et al., 2008). Still, even before observations indicated rainfall, it was realized that Titan's convective storms would likely be rare but intense relative to Earth's (Lorenz, 2000; Lorenz et al., 2005). Cloud-resolving simulations indeed predict substantial rainfall totals from deep convection amounting to tens of centimeters of

liquid (Hueso and Sánchez-Lavega, 2006; Barth and Rafkin, 2007, 2010; Rafkin et al., 2022), and recent GCM simulations likewise predict copious precipitation from infrequent storms (Schneider et al., 2012; Faulk et al., 2017; Battalio et al., 2022). For example, with the coupled GCM described in the previous section, simulated average precipitation amounts per Titan year over the wettest latitudes and precipitation amounts from individual storms are of similar magnitudes (Battalio et al., 2022)—in other words, any one location in Titan's relatively wet high latitudes might expect to see one substantial storm per Titan year (in summertime, given the average seasonality). At lower latitudes, both the average rainfall and the frequency of events are likely lower.

With a more idealized but similar model, Faulk et al. (2017) more fully quantified precipitation variability by latitude and found that, while average precipitation rates peak at the summer poles at roughly 0.1 mm d^{-1}, the maximum rates occur over the summer mid-latitudes and easily exceed 100 mm d^{-1}. These strongest storms have a recurrence interval of several Titan decades—that is, they are quite rare (Fig. 9). In addition, storms that achieve the minimum threshold estimated for erosion to happen ($\sim$10 mm d^{-1}; e.g., Perron et al., 2006) occur roughly once per Titan year at all but the highest latitudes, where weaker but frequent precipitation dominates. Indeed, the latitudinal profile of precipitation peakedness—a measure of local

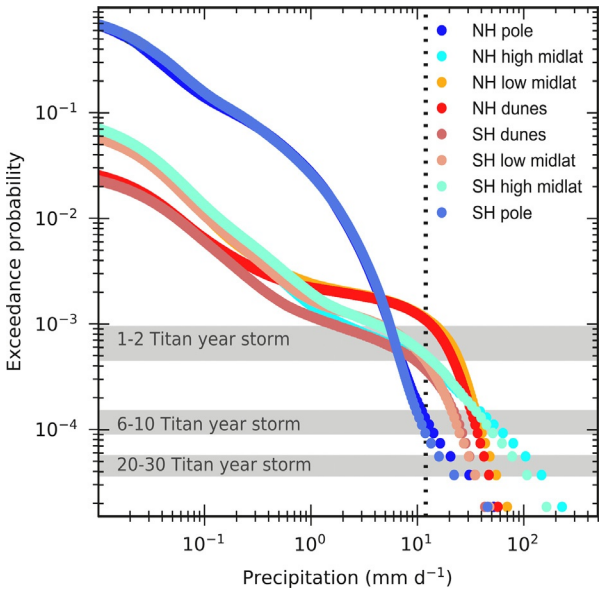

Fig. 9

Exceedance probabilities for precipitation rates in different latitude regions, calculated from precipitation simulated in a GCM. Shaded regions show the associated recurrence intervals. The *vertical dotted line* indicates the minimum precipitation rate estimated for erosion to occur (Perron et al., 2006). *Adapted from Faulk, S.P., Moon, S., Mitchell, J.L., and Lora, J.M. 2017. Regional patterns of extreme precipitation on Titan consistent with observed alluvial fan distribution. Nat. Geosci., 10, 827–831.*

variability—is correlated with the distribution of observed alluvial fans on Titan (Birch et al., 2016; Cartwright and Burr, 2017), implying a strong connection between infrequent and extreme rainstorms and a conspicuous type of alluvial geomorphic feature on Titan's surface (Faulk et al., 2017). Other landforms similarly imply latitudinal gradients in fluvial erosion occurring on Titan. Titan's impact craters, which are already relatively scarce (e.g., Hedgepeth et al., 2020), occur preferentially at lower latitudes; differential erosion rates between low and high latitudes, as described earlier, are a potential explanation (Neish et al., 2016). Titan's craters also commonly lack central peaks and pits; fluvial erosion can erase these more steeply sloped features and thus may also explain this observation (Neish et al., 2016). Channels and valleys are especially common at higher latitudes including in the extensive "labyrinth" terrain (e.g., Malaska et al., 2020), indicating fluvial activity there. And, indeed, channels at the north pole are liquid-filled (Poggiali et al., 2016), which both demonstrates the generally wetter high-latitude climate and indicates fluvial erosion is an ongoing process.

Perhaps the most difficult meteorological component to measure on Titan is the wind (Section 2.1), but its impact on the surface is widespread. Certainly near-surface winds undergo seasonal variations (Tokano, 2008; Mitchell et al., 2009; Lebonnois et al., 2012; Lora et al., 2015). The prevailing meridional flow at the lowest levels depends on the seasonal Hadley circulation (Figs. 2 and 7), and GCMs predict similar trends both at high (Lorenz et al., 2012) and low latitudes (Lora et al., 2019). However, the variability of winds in the lower atmosphere is essentially unknown from observations; estimates from GCMs indicate some variability in addition to the seasonality, with generally weak surface winds (Fig. 10), in agreement with the *Huygens* measurement and other estimates (Lora et al., 2019). Nevertheless, two types of features indirectly suggest the wind behavior: Titan's equatorial dune fields and waves on the surfaces of the polar seas.

Titan's enormous linear dunes make up vast sand seas that almost entirely encircle the equatorial region (Lorenz et al., 2006; Radebaugh et al., 2008; Lorenz and Radebaugh, 2009). These distinctive aeolian features are clear evidence that Titan's low latitudes are dry over the long term (Lorenz et al., 2006), but their existence also indicates a wind regime wherein eastward flow dominates (Radebaugh et al., 2008). This is puzzling because the atmosphere should somewhere gain positive angular momentum from the solid body to maintain its superrotation, and this occurs most reasonably via westward near-surface flow at low latitudes (e.g., Tokano, 2010); GCM simulations consistently predict generally westward equatorial surface zonal wind. Tokano (2010) suggested that the seasonally reversing meridional winds form the dunes, but eastward wind bursts are required to elongate them as observed (and cause their observed interaction with geographic obstacles; Radebaugh et al., 2008). Charnay et al. (2015) further suggested that equinoctial moist convective storms near the equator can mix down the ample angular momentum aloft, leading to westward surface gust fronts of up to 10m s^{-1} that therefore affect the dunes. This mechanism requires relatively strong wind shear to tilt the storms and may therefore be associated especially with (potentially rare) organized

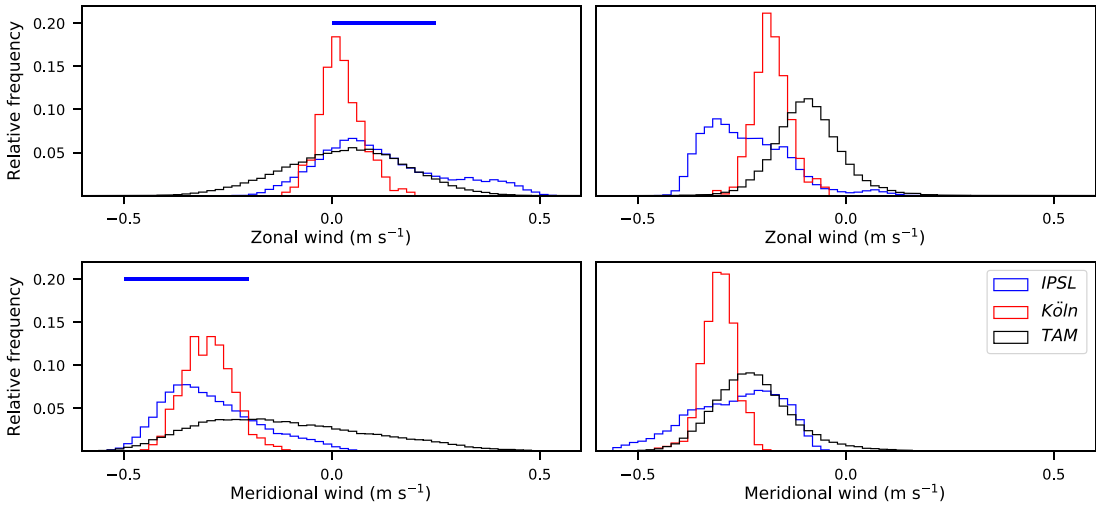

Fig. 10

Simulated wind distributions. *Left*: Histograms of diurnal average 10 m zonal (*top*) and meridional (*bottom*) winds corresponding to the season and latitude (10°S) of the *Huygens* landing, from three GCMs. *Blue bars* indicate observational estimates of winds (Lorenz et al., 2006; Karkoschka, 2007; Schröder et al., 2012); their vertical position is arbitrary. *Right*: As with left panels, but for 10°N. *Adapted from Lora, J.M., Tokano, T., Vatant d'Ollone, J., Lebonnois, S., Lorenz, R.D. 2019. A model intercomparison of Titan's climate and low-latitude environment. Icarus, 333, 113–126.*

convection (Rafkin and Barth, 2015). On the other hand, it is possible that Titan's sand grains, once initially lifted, may saltate under lower wind speeds than previously assumed, potentially increasing saltation mass fluxes (Comola et al., 2022). It is worth emphasizing that the effects of resolved convection on wind gusts have not yet been incorporated into a GCM, so mutual interactions between flow at these scales and the possible seasonality of the aforementioned mechanism remain untested. Intriguingly, however, Rodriguez et al. (2018) reported the possible detection of a dust storm at equatorial latitudes during equinox—plausibly a haboob associated with equinoctial storms. All of this certainly suggests that Titan's dunes are presently active, and points to the importance of the strongest (and rarest) surface wind gusts.

Titan's seas and lakes offer another indirect opportunity to characterize near-surface atmospheric flow via wind-driven waves on their surfaces. Of course, such features are more transient than the dunes and therefore trickier to interpret. Indeed, despite a likely relatively low threshold for wind speeds to generate capillary waves (Hayes et al., 2013), many observations indicated perfectly placid surfaces that suggested either exceptionally calm conditions or exotic characteristics of the liquid (Wye et al., 2009; Stephan et al., 2010; Barnes et al., 2011; Zebker et al., 2014; Grima et al., 2017). Lorenz et al. (2010) and Hayes et al. (2013) noted that the seasonality of winds at the polar regions, as predicted with GCMs, could be responsible for the lack of detections, and several later observations were indeed interpreted to indicate

wave-induced roughness as the north progressed into late spring (Barnes et al., 2014; Hofgartner et al., 2016). However, it is still not obvious that only the season should dictate the presence of surface waves on Titan's seas: Winds predicted by GCMs are close to expected thresholds, GCMs do not all predict similar behavior, and, most importantly, winds over the lakes are likely to be strongly affected by regional features and influenced by the seas themselves (Chatain et al., 2024; Rafkin and Soto, 2020). Therefore, whether sea surface waves probe average seasonal winds, gusts associated with atmospheric variability, and/or regional characteristics remains an open question.

4 Paleoclimate and climate evolution

As suggested in the previous sections, the mere presence of surface features like dunes, rivers, canyons, deltas, lakes, and seas implies a record of Titan's climate history. The question is whether this record is readily interpretable, and what it might tell us. The subject of Titan's climate evolution, despite being several decades old, is still in its infancy. The specific records stored in some of Titan's surface features are covered in later chapters; here, we provide an overview of our current understanding of Titan's paleoclimate.

One curious aspect of Titan's climate system as observed by *Cassini* is that it appears decidedly unstable, at least on long timescales. The photochemical lifetime of Titan's atmospheric methane is on the order of 10^7 years (Yung et al., 1984; Krasnopolsky, 2009). At the same time, isotopic measurements suggest that Titan's atmospheric nitrogen is primordial whereas the atmospheric methane is not (e.g., Mandt et al., 2009, 2012), in agreement with the hypothesis that significant methane outgassing occurred within the last billion years (Tobie et al., 2006). Other lines of evidence also point to an atmospheric age of several hundred million years (Hörst, 2017). Importantly, atmospheric methane is the photochemical precursor of both Titan's haze and its H_2, both of which are key players in radiative heating: The haze absorbs sunlight, producing Titan's stratosphere and cooling the surface (McKay et al., 1991), while the molecular hydrogen contributes opacity through collision-induced absorption with nitrogen (methane itself is also a key source of collision-induced opacity) and is therefore an important greenhouse gas (McKay et al., 1989). Thus, if methane were not resupplied to the atmosphere at a rate comparable to its loss, much of the system as observed would fall apart.

Indeed, Lorenz et al. (1997) suggested that, especially in the deep past ($\sim$3 billion years ago) when the Sun was fainter, the diminished greenhouse effect from a lack of atmospheric methane could lead to nitrogen condensation, weakening atmospheric heat transport and therefore further cooling polar regions, in turn allowing nitrogen frost, a higher albedo, and thus potentially a collapse of the atmosphere. Charnay et al. (2014) extended this idea with a GCM study, suggesting that, in a state without methane, Titan might support a nitrogen hydrologic cycle with polar liquids. Under a faint young Sun, this might extend to near-global nitrogen oceans but not, except in the case of extremely high albedo, a fully collapsed state with frozen

nitrogen. More recently, Tokano and Lorenz (2021) proposed that methane outgassing into a cold, dry atmosphere could produce a buildup of methane frost on the surface, potentially leading to a snowball state (akin to Earth's snowball episodes (e.g., Hoffman and Schrag, 2002)) as a result of ice-albedo feedback. Finally, Wong et al. (2015) suggested that, in a snowball-like state (with little methane in the atmosphere), photochemical nitrile production would dominate over hydrocarbon production, implying that the chemistry of materials deposited on the surface could reveal whether or not such a state occurred in Titan's past, at least over extended periods.

Titan's paleoclimate evolution on much shorter and more recent timescales has also received considerable attention, this time focused on the methane cycle itself. In addition to their existence, *Cassini* observations revealed that Titan's polar surface liquids are asymmetrically distributed, with the large seas and most lakes occurring in the north, and only one prominent lake in the south (Aharonson et al., 2009; Hayes, 2016). In addition, dry basins—presumably dry paleoseas—of similar area to the extant northern seas appear to exist in the south (Birch et al., 2017, 2018). All of this was hypothesized by Aharonson et al. (2009) to be a response to seasonal insolation asymmetries induced by Saturn's orbital precession—which evolves on approximately 10^4 year timescales—leading to the prediction that Titan undergoes climate cycles akin to Earth's Croll-Milankovitch cycles (Fig. 11). The idea is that seasonal insolation differences between the hemispheres cause net precipitation and thus surface accumulation differences and, therefore, over centennial or millennial timescales, net methane transport from one hemisphere to another.

Simulations with GCMs have consistently shown that surface liquids on Titan are less stable at low than at high latitudes, where they are more readily cold-trapped; therefore, equatorial liquids tend to evaporate and the atmosphere transports that methane poleward (Rannou et al., 2006; Mitchell, 2008; Schneider et al., 2012; Lora et al., 2015; Newman et al., 2016).

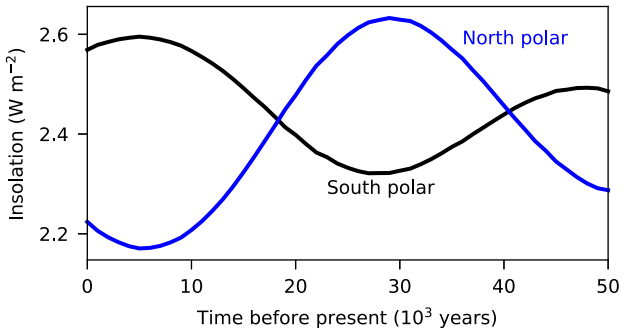

Fig. 11

Variations in annual average insolation at the top of the atmosphere at the poles (60–90° latitude), excluding polar night, going back 50,000years. These seasonal asymmetry variations are mainly due to Saturn's apsidal precession (Aharonson et al., 2009).

Furthermore, GCMs with simplified surface hydrology schemes generally simulate preferential accumulation of surface methane in the northern polar region relative to the southern under Saturn's present orbital configuration (Schneider et al., 2012; Lora et al., 2014; Newman et al., 2016), and Lora et al. (2014) additionally used such a model to demonstrate a strong linear dependence between the hemispheric surface liquid differences and the peak insolation differences under four different orbital configurations covering approximately the last 40,000 years. Finally, Lora and Mitchell (2015) demonstrated that, in one model at least, asymmetric atmospheric methane transport from south to north (under modern orbital configuration) was largely due to transport by high-latitude eddies (interacting with the seasonal cross-equatorial Hadley circulation in a "bucket brigade") that were stronger in the south than the north. This consistency implies some robustness, so these GCM results lend credence to the orbital forcing hypothesis.

However, the situation on Titan may be more subtle than implied by the results mentioned above. First, the aforementioned simulations did not produce the dramatic (roughly 10-to-1) north-to-south modern asymmetry observed (Aharonson et al., 2009); instead, they predict that the north should have at most twice as much methane (Schneider et al., 2012; Lora et al., 2014; Newman et al., 2016). Second, observed putative evaporites are widespread in the northern basins and shores of filled lakes, but their absence from the southern polar surface is conspicuous (MacKenzie et al., 2014). A possible explanation is that southern evaporites have been buried or eroded on millennial timescales; an alternative is that they did not form in the first place. Third, more recent GCM results indicate that surface heterogeneities and surface hydrology complicate the story: Tokano (2019) found that, in a model without surface hydrology, heterogeneous topography caused a buildup of methane in the north, and this swamped any signal from orbital forcing (though, in this model, the asymmetry *without* topography was reversed, even for modern orbital configuration, leading to slightly more methane in the south). And, most recently, Lora et al. (2022) found that, in a coupled model incorporating active land hydrology (Faulk et al., 2020) both with and without topography, the surface liquid distribution did not respond strongly to orbital forcing. Interestingly, this model did simulate net atmospheric methane transport consistent with prior results (Lora et al., 2014; Lora and Mitchell, 2015), once again indicating that the orbital forcing mechanism is *possible*; however, this transport did not directly lead to surface liquid asymmetries, meaning it was of secondary importance relative to the effects of surface hydrology.

Thus, whether or not Titan's methane cycle undergoes orbitally paced variations that leave a record on the surface remains to be determined. Interestingly, the morphology of dunes at lower latitudes suggests changes in winds and sediment availability, and the timescale for their reorientation may be similar to that of orbital precession (Ewing et al., 2015; McDonald et al., 2016). Therefore, Titan's dune fields could be independent archives of its climate cycles. Still, observations of the surface allow conflicting interpretations, as do GCM simulations. Of high importance, especially for the latter, will be an improved understanding of Titan's surface

properties and better, more complete knowledge of Titan's topography. If the lakes and seas are undergoing secular—as opposed to merely seasonal—changes such as shoreline retreat, the regional details are likely to matter. All of this points to the need for future missions. Titan's climate has all the potential to evolve; the question is whether or not that evolution is ongoing and detectable.

5 Conclusion

Cassini-Huygens revealed Titan's climate system to be active and complex, in many ways more so than previously expected. In part due to its connection to the surface, Titan's lower atmosphere is highly dynamic despite being cold and massive: Contrasting climates at high and low latitudes undergo strong seasonal changes; clouds and storms are relatively common features, many organized by a diverse family of atmospheric waves; rain and wind sculpt Titan's varied surface, which thus may hold clues to the history of the climate. Much progress has been made through observations, laboratory experiments, and modeling, and we now recognize Titan as Earth's eccentric sibling—exotic and unique, but at the same time eerily similar.

Naturally, our increasing understanding has come with a torrent of new questions. The sections of this chapter have hinted at a few categories of future inquiry relevant to Titan's weather and climate. For example, much remains unknown about the clouds: Which precipitate, and how are they organized? Are some directly coupled to surface features as orographic clouds, lake-effect clouds, or fog? Do high-altitude cirrus explain the discrepant observations at shorter and longer wavelengths? Similarly, the surface and its role in the climate remain opaque: What are its hydraulic properties? How much methane exists in subsurface reservoirs, what is their global distribution, and how are they connected to the atmosphere? Why was the surface at the *Huygens* landing site seemingly moist (Niemann et al., 2005)? And, finally, even a number of big-picture questions remain unanswered: What is the climate variability, from subseasonal to interannual? How has paleoclimate influenced the surface? What is the role of the (seemingly missing) ethane?

Further inquiry will need new and increasingly targeted data. Continued ground-based telescopic monitoring (e.g., Corlies et al., 2019) and future observations with facilities such as the James Webb Space Telescope (Nixon et al., 2016) will provide further insights into the seasonal patterns of Titan's weather, as ongoing theoretical and modeling investigations focus understanding of relevant processes. But many outstanding lines of inquiry—like how Titan's atmosphere, surface, and interior are linked (MacKenzie et al., 2021)—await essential information that will require future missions. *Dragonfly*, whose science goals include better understanding how the equatorial deserts fit into the global methane cycle and investigating the processes that modify the surface, among many other critical advances (Barnes et al., 2021), is a remarkable continuation of Titan exploration. Research into Titan's weather, climate, and paleoclimate in the coming decades, following up on the legacy of *Cassini-Huygens*, promises to provide another fundamental transformation in our understanding of this fascinating world.

Acknowledgments

We gratefully acknowledge T. Tokano, S. Lebonnois, and J. M. Battalio for constructive comments that helped to clarify aspects of the text.

References

Achterberg, R.K., Conrath, B.J., Gierasch, P.J., Flasar, F.M., Nixon, C.A., 2008. Titan's middle-atmospheric temperatures and dynamics observed by the Cassini Composite Infrared Spectrometer. Icarus 194, 263–277.

Achterberg, R.K., Gierasch, P.J., Conrath, B.J., Flasar, F.M., Nixon, C.A., 2011. Temporal variations of Titan's middle-atmospheric temperatures from 2004 to 2009 observed by Cassini/CIRS. Icarus 211, 686–698.

Ádámkovics, M., Barnes, J.W., Hartung, M., de Pater, I., 2010. Observations of a stationary mid-latitude cloud system on Titan. Icarus 208, 868–877.

Ádámkovics, M., Mitchell, J.L., Hayes, A.G., Rojo, P.M., Corlies, P., Barnes, J.W., Ivanov, V.D., Brown, R.H., Baines, K.H., Buratti, B.J., Clark, R.N., Nicholson, P.D., Sotin, C., 2016. Meridional variation in tropospheric methane on Titan observed with AO spectroscopy at Keck and VLT. Icarus 270, 376–388.

Aharonson, O., Hayes, A.G., Lunine, J.I., Lorenz, R.D., Allison, M.D., Elachi, C., 2009. An asymmetric distribution of lakes on Titan as a possible consequence of orbital forcing. Nat. Geosci. 2, 851–854.

Awal, M., Lunine, J.I., 1994. Moist convective clouds in Titan's atmosphere. Geophys. Res. Lett. 21, 2491–2494.

Barnes, J.W., Soderblom, J.M., Brown, R.H., Soderblom, L.A., Stephan, K., Jaumann, R., Le Mouélic, S., Rodriguez, S., Sotin, C., Buratti, B.J., Baines, K.H., Clark, R.N., Nicholson, P.D., 2011. Wave constraints for Titan's Jingpo Lacus and Kraken Mare from VIMS specular reflection lightcurves. Icarus 211, 722–731.

Barnes, J.W., Buratti, B.J., Turtle, E.P., Bow, J., Dalba, P.A., Perry, J., Brown, R.H., Rodriguez, S., Mouélic, S.L., Baines, K.H., Sotin, C., Lorenz, R.D., Malaska, M.J., McCord, T.B., Clark, R.N., Jaumann, R., Hayne, P.O., Nicholson, P.D., Soderblom, J.M., Soderblom, L.A., 2013. Precipitation-induced surface brightenings seen on Titan by Cassini VIMS and ISS. Planet. Sci. 2, 1.

Barnes, J.W., Sotin, C., Soderblom, J.M., Brown, R.H., Hayes, A.G., Donelan, M., Rodriguez, S., Le Mouélic, S., Baines, K.H., McCord, T.B., 2014. Cassini/VIMS observes rough surfaces on Titan's Punga Mare in specular reflection. Planet. Sci. 3, 3.

Barnes, J.W., Turtle, E.P., Trainer, M.G., Lorenz, R.D., MacKenzie, S.M., Brinckerhoff, W.B., Cable, M.L., Ernst, C.M., Freissinet, C., Hand, K.P., Hayes, A.G., Hörst, S.M., Johnson, J.R., Karkoschka, E., Lawrence, D.J., Gall, A.L., Lora, J.M., McKay, C.P., Miller, R.S., Murchie, S.L., Neish, C.D., Newman, C.E., Núñez, J., Panning, M.P., Parsons, A.M., Peplowski, P.N., Quick, L.C., Radebaugh, J., Rafkin, S.C.R., Shiraishi, H., Soderblom, J.M., Sotzen, K.S., Stickle, A.M., Stofan, E.R., Szopa, C., Tokano, T., Wagner, T., Wilson, C., Yingst, R.A., Zacny, K., Stähler, S.C., 2021. Science goals and objectives for the Dragonfly Titan rotorcraft relocatable lander. Planet. Sci. J. 2, 130.

Barth, E.L., 2010. Cloud formation along mountain ridges on Titan. Planet. Space Sci. 13, 1740–1747.

Barth, E.L., Rafkin, S.C.R., 2007. TRAMS: A new dynamic cloud model for Titan's methane clouds. Geophys. Res. Lett. 34, L03203.

Barth, E.L., Rafkin, S.C.R., 2010. Convective cloud heights as a diagnostic for methane environment on Titan. Icarus 206, 467–484.

Battalio, J.M., Lora, J.M., 2021a. Annular modes of variability in the atmospheres of Mars and Titan. Nature Astronomy 5, 1139–1147.

Battalio, J.M., Lora, J.M., 2021b. Global impacts from high-latitude storms on Titan. Geophys. Res. Lett. 48, e2021GL094244.

Battalio, J.M., Lora, J.M., Rafkin, S., Soto, A., 2022. The interaction of deep convection with the general circulation in Titan's atmosphere. Part 2: Impacts on the climate. Icarus 373, 114623.

Bézard, B., Vinatier, S., Achterberg, R.K., 2018. Seasonal radiative modeling of Titan's stratospheric temperatures at low latitudes. Icarus 302, 437–450.

Birch, S.P.D., Hayes, A.G., Howard, A.D., Moore, J.M., Radebaugh, J., 2016. Alluvial fan morphology, distribution and formation on Titan. Icarus 270, 238–247.

Birch, S.P.D., Hayes, A.G., Dietrich, W.E., Howard, A.D., Bristow, C.S., Malaska, M.J., Moore, J.M., Mastrogiuseppe, M., Hofgartner, J.D., Williams, D.A., White, O.H., Soderblom, J.M., Barnes, J.W., Turtle, E.P., Lunine, J.I., Wood, C.A., Neish, C.D., Kirk, R.L., Stofan, E.R., Lorenz, R.D., Lopes, R.M.C., 2017. Geomorphologic mapping of Titan's polar terrains: Constraining surface processes and landscape evolution. Icarus 282, 214–236.

Birch, S.P.D., Hayes, A.G., Corlies, P., Stofan, E.R., Hofgartner, J.D., Lopes, R.M.C., Lorenz, R.D., Lunine, J.I., MacKenzie, S.M., Malaska, M.J., Woode, C.A., the Cassini RADAR Team, 2018. Morphological evidence that Titan's southern hemisphere basins are paleoseas. Icarus 310, 140–148.

Bird, M.K., Allison, M., Asmar, S.W., Atkinson, D.H., Avruch, I.M., Dutta-Roy, R., Dzierma, Y., Edenhofer, P., Folkner, W.M., Gurvits, L.I., Johnston, D.V., Plettemeier, D., Pogrebenko, S.V., Preston, R.A., Tyler, G.L., 2005. The vertical profile of winds on Titan. Nature 438, 800–802.

Bouchez, A.H., Brown, M.E., 2005. Statistics of Titan's south polar tropospheric clouds. Astrophys. J. 618, L53–L56.

Broadfoot, A.L., Sandel, B.R., Shemansky, D.E., Holberg, J.B., Smith, G.R., Strobel, D.F., McConnell, J.C., Kumard, S., Hunten, D.M., Atreya, S.K., Donahue, T.M., Moos, H.W., Bertaux, J.L., Blamont, J.E., Pomphrey, R.B., Lunick, S., 1981. Extreme ultraviolet observations from Voyager 1 encounter with Saturn. Science 212, 206–211.

Brown, M.E., Bouchez, A.H., Griffith, C.A., 2002. Direct detection of variable tropospheric clouds near Titan's south pole. Nature 420, 795–797.

Brown, R.H., Baines, K.H., Bellucci, G., Bibring, J., Buratti, B.J., Capaccioni, F., Cerroni, P., Clark, R.N., Coradini, A., Cruikshank, D.P., Drossart, P., Formisano, V., Jaumann, R., Langevin, Y., Matson, D.L., McCord, T.B., Mennella, V., Miller, E., Nelson, R.M., Nicholson, P.D., Sicardy, B., Sotin, C., 2004. The Cassini Visual and Infrared Mapping Spectrometer (VIMS) investigation. Space Sci. Rev. 115, 111–168.

Brown, M.E., Schaller, E.L., Roe, H.G., Chen, C., Roberts, J., Brown, R.H., Baines, K.H., Clark, R.N., 2009a. Discovery of lake-effect clouds on Titan. Geophys. Res. Lett. 36, L01103.

Brown, M.E., Smith, A.L., Chen, C., Ádámkovics, M., 2009b. Discovery of fog at the South Pole of Titan. Astrophys. J. Lett. 706, L110–L113.

Burr, D.M., Perron, J.T., Lamb, M.P., Irwin, R.P., Collins, G.C., Howard, A.D., Sklar, L.S., Moore, J.M., Ádámkovics, M., Baker, V.R., Drummond, S.A., Black, B.A., 2013. Fluvial features on Titan: Insights from morphology and modeling. Geol. Soc. Am. Bull. 125, 299–321.

Cartwright, R., Burr, D., 2017. Using synthetic aperture radar data of terrestrial analogs to test for alluvial fan formation mechanisms on Titan. Icarus 284, 183–205.

Charnay, B., Lebonnois, S., 2012. Two boundary layers in Titan's lower troposphere inferred from a climate model. Nat. Geosci. 5, 106–109.

Charnay, B., Forget, F., Tobie, G., Sotin, C., Wordsworth, R., 2014. Titan's past and future: 3D modeling of a pure nitrogen atmosphere and geological implications. Icarus 241, 269–279.

Charnay, B., Barth, E., Rafkin, S., Narteau, C., Lebonnois, S., Rodriguez, S., Courrech du Pont, S., Lucas, A., 2015. Methane storms as a driver of Titan's dune orientation. Nat. Geosci. 8, 362–366.

Chatain, A., Rafkin, S.C.R., Soto, A., Moisan, E., Lora, J.M., Le Gall, A., Hueso, R., Spiga, A., 2024. The impact of lake shape and size on lake breezes and air–lake exchanges on Titan. Icarus. 411, 115925.

Comola, F., Kok, J.F., Lora, J.M., Cohanim, K., Yu, X., He, C., McGuiggan, P., Hörst, S.M., Turney, F., 2022. Titan's prevailing circulation might drive highly intermittent, yet significant sediment transport. Geophys. Res. Lett. 49, e2022GL097913.

Corlies, P., Hayes, A., Birch, S., Lorenz, R., Stiles, B., Kirk, R., Poggiali, V., Zebker, H., Iess, L., 2017. Titan's topography and shape at the end of the Cassini Mission. Geophys. Res. Lett. 44, 11754–11761.

Corlies, P., Hayes, A.G., Kelland, J., Ádámkovics, M., Rodriguez, S., Rojo, P., Turtle, E.P., Lora, J., Mitchell, J., Lunine, J., Perry, J.E., 2019. Ongoing monitoring of clouds on Titan. In: 50th Annual Lunar and Planetary Science Conference, Lunar and Planetary Science Conferencep. 2776.

Corlies, P., Hayes, A., Soto, A., Lora, J., Soderblom, J., Adamkovics, M., Turtle, E., Rodriguez, S., Mitchell, J., Johnson, A., Steckloff, J., Rojo, P., Battalio, J., 2022. Reoccurring cloud events at Titan's northern mid-latitudes. Planet. Sci. J. under review.

Cottini, V., Nixon, C.A., Jennings, D.E., de Kok, R., Teanby, N.A., Irwin, P.G.J., Flasar, F.M., 2012. Spatial and temporal variations in Titan's surface temperatures from Cassini CIRS observations. Planet. Space Sci. 60, 62–71.

Courtin, R., Kim, S.J., 2002. Mapping of Titan's tropopause and surface temperatures from Voyager IRIS spectra. Planet. Space Sci. 50, 309–321.

Dhingra, R.D., Barnes, J.W., Brown, R.H., Burrati, B.J., Sotin, C., Nicholson, P.D., Baines, K.H., Clark, R.N., Soderblom, J.M., Jauman, R., Rodriguez, S., Mouélic, S.L., Turtle, E.P., Perry, J.E., Cottini, V., Jennings, D.E., 2019. Observational evidence for summer rainfall at Titan's North Pole. Geophys. Res. Lett. 46, 1205–1212.

Dhingra, R.D., Barnes, J.W., Heslar, M.F., Brown, R.H., Buratti, B.J., Sotin, C., Soderblom, J.M., Rodriguez, S., Le Mouélic, S., Nicholson, P.D., Baines, K.H., Clark, R.N., Jaumann, R., 2020. Spatio-temporal variation of bright ephemeral features on Titan's north pole. Planet. Sci. J. 1, 31.

Ewing, R.C., Hayes, A.G., Lucas, A., 2015. Sand dune patterns on Titan controlled by long-term climate cycles. Nat. Geosci. 8, 15–19.

Faulk, S.P., Moon, S., Mitchell, J.L., Lora, J.M., 2017. Regional patterns of extreme precipitation on Titan consistent with observed alluvial fan distribution. Nat. Geosci. 10, 827–831.

Faulk, S.P., Lora, J.M., Mitchell, J.L., Milly, P.C.D., 2020. Titan's climate patterns and surface methane distribution due to the coupling of land hydrology and atmosphere. Nat. Astron. 4, 390–398.

Flasar, F.M., Achterberg, R.K., 2009. The structure and dynamics of Titan's middle atmosphere. Philos. Trans. A Math. Phys. Eng. Sci. 367, 649–664.

Flasar, F.M., Samuelson, R.E., Conrath, B.J., 1981. Titan's atmosphere: temperature and dynamics. Nature 292, 693–698.

Flasar, F.M., Achterberg, R.K., Conrath, B.J., Gierasch, P.J., Kunde, V.G., Nixon, C.A., Bjoraker, G.L., Jennings, D.E., Romani, P.N., Simon-Miller, A.A., Bézard, B., Coustenis, A., Irwin, P.G.J., Teanby, N.A., Brasunas, J., Pearl, J.C., Segura, M.E., Carlson, R.C., Mamoutkine, A., Schinder, P.J., Barucci, A., Courtin, R., Fouchet, T., Gautier, D., Lellouch, E., Marten, A., Prangé, R., Vinatier, S., Strobel, D.F., Calcutt, S.B., Read, P.L., Taylor, F.W., Bowles, N., Samuelson, R.E., Orton, G.S., Spilker, L.J., Owen, T.C., Spencer, J.R., Showalter, M.R., Ferrari, C., Abbas, M.M., Raulin, F., Edgington, S., Ade, P., Wishnow, E.H., 2005. Titan's atmospheric temperatures, winds, and composition. Science 308, 975–978.

Flasar, F.M., Achterberg, R.K., Schinder, P.J., 2014. Thermal structure of Titan's troposphere and middle atmosphere. In: Müller-Wodarg, I., Griffith, C.A., Lellouch, E., Cravens, T.E. (Eds.), Titan: Interior, surface, atmosphere, and space environment. Cambridge University Press, Cambridge, pp. 102–121.

Fulchignoni, M., Ferri, F., Angrilli, F., Ball, A.J., Bar-Nun, A., Barucci, M.A., Bettanini, C., Bianchini, G., Borucki, W., Colombatti, G., Coradini, M., Coustenis, A., Debei, S., Falkner, P., Fanti, G., Flamini, E., Gaborit, V., Grard, R., Hamelin, M., Harri, A.M., Hathi, B., Jernej, I., Leese, M.R., Lehto, A., Lion Stoppato, P.F., López-Moreno, J.J., Mäkinen, T., McDonnell, J.A.M., McKay, C.P., Molina-Cuberos, G., Neubauer, F.M., Pirronello, V., Rodrigo, R., Saggin, B., Schwingenschuh, K., Seiff, A., Simões, F., Svedhem, H., Tokano, T., Towner, M.C., Trautner, R., Withers, P., Zarnecki, J.C., 2005. In situ measurements of the physical characteristics of Titan's environment. Nature 438, 785–791.

Graves, S.D.B., McKay, C.P., Griffith, C.A., Ferri, F., Fulchignoni, M., 2008. Rain and hail can reach the surface of Titan. Planet. Space Sci. 56, 346–357.

Griffith, C.A., Owen, T., Miller, G.A., Geballe, T., 1998. Transient clouds in Titan's lower atmosphere. Nature 395, 575–578.

Griffith, C.A., Hall, J.L., Geballe, T.R., 2000. Detection of daily clouds on Titan. Science 290, 509–513.

Griffith, C.A., Penteado, P., Baines, K., Drossart, P., Barnes, J., Bellucci, G., Bibring, J., Brown, R., Buratti, B., Capaccioni, F., Cerroni, P., Clark, R., Combes, M., Coradini, A., Cruikshank, D., Formisano, V., Jaumann, R., Langevin, Y., Matson, D., McCord, T., Mennella, V., Nelson, R., Nicholson, P., Sicardy, B., Sotin, C., Soderblom, L.A., Kursinski, R., 2005. The evolution of Titan's mid-latitude clouds. Science 310, 474–477.

Griffith, C.A., Penteado, P., Rannou, P., Brown, R., Boudon, V., Baines, K.H., Clark, R., Drossart, P., Buratti, B., Nicholson, P., McKay, C.P., Coustenis, A., Negrao, A., Jaumann, R., 2006. Evidence for a polar ethane cloud on Titan. Science 313, 1620–1622.

Griffith, C.A., McKay, C.P., Ferri, F., 2008. Titan's tropical storms in an evolving atmosphere. Astrophys. J. 687, L41–L44.

Griffith, C.A., Rafkin, S., Rannou, P., McKay, C.P., 2014. Storms, clouds, and weather. In: Müller-Wodarg, I., Griffith, C.A., Lellouch, E., Cravens, T.E. (Eds.), Titan: Interior, Surface, Atmosphere, and Space Environment. Cambridge University Press, Cambridge, pp. 190–223.

Grima, C., Mastrogiuseppe, M., Hayes, A.G., Wall, S.D., Lorenz, R.D., Hofgartner, J.D., Stiles, B., Elachi, C., the Cassini RADAR Team, 2017. Surface roughness of Titan's hydrocarbon seas. Earth Planet. Sci. Lett. 474, 20–24.

Hayes, A.G., 2016. The lakes and seas of Titan. Annu. Rev. Earth Planet. Sci. 44, 57–83.

Hayes, A., Aharonson, O., Callahan, P., Elachi, C., Gim, Y., Kirk, R., Lewis, K., Lopes, R., Lorenz, R., Lunine, J., Mitchell, K., Mitri, G., Stofan, E., Wall, S., 2008. Hydrocarbon lakes on Titan: Distribution and interaction with a porous regolith. Geophys. Res. Lett. 35, L09204.

Hayes, A.G., Lorenz, R.D., Donelan, M.A., Manga, M., Lunine, J.I., Schneider, T., Lamb, M.P., Mitchell, J.M., Fischer, W.W., Graves, S.D., Tolman, H.L., Aharonson, O., Encrenaz, P.J., Ventura, B., Casarano, D., Notarnicola, C., 2013. Wind driven capillary-gravity waves on Titan's lakes: Hard to detect or non-existent? Icarus 225, 403–412.

Hayes, A.G., Birch, S.P.D., Dietrich, W.E., Howard, A.D., Kirk, R.L., Poggiali, V., Mastrogiuseppe, M., Michaelides, R.J., Corlies, P.M., Moore, J.M., Malaska, M.J., Mitchell, K.L., Lorenz, R.D., Wood, C.A., 2017. Topographic constraints on the evolution and connectivity of Titan's lacustrine basins. Geophys. Res. Lett. 44, 11745–11753.

Hayes, A.G., Lorenz, R.D., Lunine, J.I., 2018. A post-Cassini view of Titan's methane-based hydrologic cycle. Nat. Geosci. 11, 306–313.

Hedgepeth, J.E., Neish, C.D., Turtle, E.P., Stiles, B.W., Kirk, R., Lorenz, R.D., 2020. Titan's impact crater population after Cassini. Icarus. 344, 113664.

Hoffman, P.F., Schrag, D.P., 2002. The snowball Earth hypothesis: testing the limits of global change. Terra Nova 14, 129–155.

Hofgartner, J.D., Hayes, A.G., Lunine, J.I., Zebker, H., Lorenz, R.D., Malaska, M.J., Mastrogiuseppe, M., Notarnicola, C., Soderblom, J.M., 2016. Titan's "magic islands": transient features in a hydrocarbon sea. Icarus 271, 338–349.

Hörst, S.M., 2017. Titan's atmosphere and climate. J. Geophys. Res. Planets 122, 432–482.

Horvath, D.G., Andrews-Hanna, J.C., Newman, C.E., Mitchell, K.L., Stiles, B.W., 2016. The influence of subsurface flow on lake formation and north polar lake distribution on Titan. Icarus 277, 103–124.

Hoskins, B.J., 1982. The mathematical theory of frontogenesis. Annu. Rev. Fluid Mech. 14, 131–151.

Hourdin, F., Talagrand, O., Sadourny, R., Courtin, R., Gautier, D., McKay, C.P., 1995. Numerical simulations of the general circulation of the atmosphere of Titan. Icarus 117, 358–374.

Hueso, R., Sánchez-Lavega, A., 2006. Methane storms on Saturn's moon Titan. Nature 442, 428–431.

Janssen, M.A., Le Gall, A., Lopes, R.M., Lorenz, R.D., Malaska, M.J., Hayes, A.G., Neish, C., Solomonidou, A., Mitchell, K., Radebaugh, J., Keihm, S.J., Choukroun, M., Leyrat, C., Encrenaz, P.J., Mastrogiuseppe, M., 2016. Titan's surface at 2.18-cm wavelength imaged by the Cassini RADAR radiometer: Results and interpretations through the first ten years of observation. Icarus 270, 443–459.

Jaumann, R., Brown, R.H., Stephan, K., Barnes, J.W., Soderblom, L.A., Sotin, C., Le Mouélic, S., Clark, R.N., Soderblom, J., Buratti, B.J., Wagner, R., McCord, T.B., Rodriguez, S., Baines, K.H., Cruikshank, D.P., Nicholson, P.D., Griffith, C.A., Langhans, M., Lorenz, R.D., 2008. Fluvial erosion and post-erosional processes on Titan. Icarus 197, 526–538.

Jennings, D.E., Flasar, F.M., Kunde, V.G., Samuelson, R.E., Pearl, J.C., Nixon, C.A., Carlson, R.C., Mamoutkine, A.A., Brasunas, J.C., Guandique, E., Achterberg, R.K., Bjoraker, G.L., Romani, P.N.,

Segura, M.E., Albright, S.A., Elliott, M.H., Tingley, J.S., Calcutt, S., Coustenis, A., Courtin, R., 2009. Titan's surface brightness temperatures. Astrophys. J. 691, L103–L105.
Jennings, D.E., Cottini, V., Nixon, C.A., Flasar, F.M., Kunde, V.G., Samuelson, R.E., Romani, P.N., Hesman, B.E., Carlson, R.C., Gorius, N.J.P., Coustenis, A., Tokano, T., 2011. Seasonal changes in Titan's surface temperatures. Astrophys. J. 737, L15.
Jennings, D.E., Cottini, V., Nixon, C.A., Achterberg, R.K., Flasar, F.M., Kunde, V.G., Romani, P.N., Samuelson, R.E., Mamoutkine, A., Gorius, N.J.P., Coustenis, A., Tokano, T., 2016. Surface temperatures on Titan during northern winter and spring. Astrophys. J. Lett. 816, L17.
Jennings, D.E., Tokano, T., Cottini, V., Nixon, C.A., Achterberg, R.K., Flasar, F.M., Kunde, V.G., Romani, P.N., Samuelson, R.E., Segura, M.E., Gorius, N.J.P., Guandique, E., Kaelberer, M.S., Coustenis, A., 2019. Titan surface temperatures during the Cassini mission. Astrophys. J. Lett. 877, L8.
Karkoschka, E., 2007. DISR imaging and the geometry of the descent of the Huygens probe within Titan's atmosphere. Planet. Space Sci. 55, 1896–1935.
Karkoschka, E., 2016. Titan's meridional wind profile and Huygens' orientation and swing inferred from the geometry of DISR imaging. Icarus 270, 326–338.
Kiladis, G.N., Wheeler, M.C., Haertel, P.T., Straub, K.H., Roundy, P.E., 2009. Convectively coupled equatorial waves. Rev. Geophys. 47, 1–42.
Krasnopolsky, V.A., 2009. A photochemical model of Titan's atmosphere and ionosphere. Icarus 201, 226–256.
Kuiper, G.P., 1944. Titan: a satellite with an atmosphere. Astrophys. J. 100, 378.
Langhans, M.H., Jaumann, R., Stephan, K., Brown, R.H., Buratti, B.J., Clark, R.N., Baines, K.H., Nicholson, P.D., Lorenz, R.D., Soderblom, L.A., Soderblom, J.M., Sotin, C., Barnes, J.W., Nelson, R., 2012. Titan's fluvial valleys: Morphology, distribution, and spectral properties. Planet. Space Sci. 60, 34–51.
Lebonnois, S., Burgalat, J., Rannou, P., Charnay, B., 2012. Titan global climate model: A new 3-dimensional version of the IPSL Titan GCM. Icarus 218, 707–722.
Lebonnois, S., Flasar, F.M., Tokano, T., Newman, C.E., 2014. The general circulation of Titan's lower and middle atmosphere. In: Müller-Wodarg, I., Griffith, C.A., Lellouch, E., Cravens, T.E. (Eds.), Titan: Interior, surface, Atmosphere, and Space Environment. Cambridge University Press, Cambridge, pp. 122–157.
Lemmon, M.T., Lorenz, R.D., Smith, P.H., Caldwell, J.J., 2019. Large-scale, sub-tropical cloud activity near Titan's 1995 equinox. Icarus 331, 1–14.
Lindal, G.F., Wood, G.E., Hotz, H.B., Sweetnam, D.N., Eshleman, V.R., Tyler, G.L., 1983. The atmosphere of Titan—an analysis of the Voyager 1 radio occultation measurements. Icarus 53, 348–363.
Lora, J.M., Ádámkovics, M., 2017. The near-surface methane humidity on Titan. Icarus 286, 270–279.
Lora, J.M., Mitchell, J.L., 2015. Titan's asymmetric lake distribution mediated by methane transport due to atmospheric eddies. Geophys. Res. Lett. 42, 6213–6220.
Lora, J.M., Goodman, P.J., Russell, J.L., Lunine, J.I., 2011. Insolation in Titan's troposphere. Icarus 216, 116–119.
Lora, J.M., Lunine, J.I., Russell, J.L., Hayes, A.G., 2014. Simulations of Titan's paleoclimate. Icarus 243, 264–273.
Lora, J.M., Lunine, J.I., Russell, J.L., 2015. GCM simulations of Titan's middle and lower atmosphere and comparison to observations. Icarus 250, 516–528.
Lora, J.M., Tokano, T., Vatant d'Ollone, J., Lebonnois, S., Lorenz, R.D., 2019. A model intercomparison of Titan's climate and low-latitude environment. Icarus 333, 113–126.
Lora, J.M., Battalio, J.M., Yap, M., Baciocco, C., 2022. Topographic and orbital forcing of Titan's hydroclimate. Icarus. 384, 115095.
Lorenz, R.D., 1993. The life, death and afterlife of a raindrop on Titan. Planet. Space Sci. 41, 647–655.
Lorenz, R.D., 2000. The weather on Titan. Science 290, 467–468.
Lorenz, R.D., Lunine, J.I., 1996. Erosion on Titan: Past and present. Icarus 122, 79–91.
Lorenz, R.D., Radebaugh, J., 2009. Global pattern of Titan's dunes: Radar survey from the Cassini prime mission. Geophys. Res. Lett. 36, L03202.
Lorenz, R.D., MacKay, C.P., Lunine, J.I., 1997. Photochemically driven collapse of Titan's atmosphere. Science 275, 642–644.

Lorenz, R.D., Griffith, C.A., Lunine, J.I., McKay, C.P., Rennò, N.O., 2005. Convective plumes and the scarcity of Titan's clouds. Geophys. Res. Lett. 32, L01201.

Lorenz, R.D., Wall, S., Radebaugh, J., Boubin, G., Reffet, E., Janssen, M., Stofan, E., Lopes, R., Kirk, R., Elachi, C., Lunine, J., Mitchell, K., Paganelli, F., Soderblom, L., Wood, C., Wye, L., Zebker, H., Anderson, Y., Ostro, S., Allison, M., Boehmer, R., Callahan, P., Encrenaz, P., Ori, G.G., Francescetti, G., Gim, Y., Hamilton, G., Hensley, S., Johnson, W., Kelleher, K., Muhleman, D., Picardi, G., Posa, F., Roth, L., Seu, R., Shaffer, S., Stiles, B., Vetrella, S., Flamini, E., West, R., 2006. The sand seas of Titan: Cassini RADAR observations of longitudinal dunes. Science 312, 724–727.

Lorenz, R.D., Lopes, R.M., Paganelli, F., Lunine, J.I., Kirk, R.L., Mitchell, K.L., Soderblom, L.A., Stofan, E.R., Ori, G., Myers, M., Miyamoto, H., Radebaugh, J., Stiles, B., Wall, S.D., Wood, C.A., 2008a. Titan's inventory of organic surface materials. Geophys. Res. Lett. 35, L02206.

Lorenz, R.D., Mitchell, K.L., Kirk, R.L., Hayes, A.G., Aharonson, O., Zebker, H.A., Paillou, P., Radebaugh, J., Lunine, J.I., Janssen, M.A., Wall, S.D., Lopes, R.M., Stiles, B., Ostro, S., Mitri, G., Stofan, E.R., 2008b. Fluvial channels on Titan: Initial Cassini RADAR observations. Planet. Space Sci. 56, 1132–1144.

Lorenz, R.D., Newman, C., Lunine, J.I., 2010. Threshold of wave generation on Titan's lakes and seas: Effect of viscosity and implications for Cassini observations. Icarus 207, 932–937.

Lorenz, R.D., Newman, C.E., Tokano, T., Mitchell, J.L., Charnay, B., Lebonnois, S., Achterberg, R.K., 2012. Formulation of a wind specification for Titan late polar summer exploration. Planet. Space Sci. 70, 73–83.

Lorenz, R.D., Stiles, B.W., Aharonson, O., Lucas, A., Hayes, A.G., Kirk, R.L., Zebker, H.A., Turtle, E.P., Neish, C.D., Stofan, E.R., Barnes, J.W., the Cassini RADAR team, 2013. A global topographic map of Titan. Icarus 225, 367–377.

Lunine, J.I., Atreya, S.K., 2008. The methane cycle on Titan. Nat. Geosci. 1, 159–164.

Lunine, J.I., Lorenz, R.D., 2009. Rivers, lakes, dunes, and rain: Crustal processes in Titan's methane cycle. Annu. Rev. Earth Planet. Sci. 37, 299–320.

Lunine, J.I., Stevenson, D.J., Yung, Y.L., 1983. Ethane ocean on Titan. Science 222, 1229–1230.

MacKenzie, S.M., Barnes, J.W., Sotin, C., Soderblom, J.M., Le Mouélic, S., Rodriguez, S., Baines, K.H., Buratti, B.J., Clark, R.N., Nicholson, P.D., McCord, T.B., 2014. Evidence of Titan's climate history from evaporite distribution. Icarus 243, 191–207.

MacKenzie, S.M., Lora, J.M., Lorenz, R.D., 2019. A thermal inertia map of Titan. J. Geophys. Res. Planets 124, 1728–1742.

MacKenzie, S.M., Birch, S.P.D., Hörst, S., Sotin, C., Barth, E., Lora, J.M., Trainer, M.G., Corlies, P., Malaska, M.J., Sciamma-O'Brien, E., Thelen, A.E., Turtle, E., Radebaugh, J., Hanley, J., Solomonidou, A., Newman, C., Regoli, L., Rodriguez, S., Seignovert, B., Hayes, A.G., Journaux, B., Steckloff, J., Nna-Mvondo, D., Cornet, T., Palmer, M.Y., Lopes, R.M.C., Vinatier, S., Lorenz, R., Nixon, C., Czaplinski, E., Barnes, J.W., Sittler, E., Coates, A., 2021. Titan: Earth-like on the outside, Ocean World on the inside. Planet. Sci. J. 2, 112.

Malaska, M.J., Radebaugh, J., Lopes, R.M.C., Mitchell, K.L., Verlander, T., Schoenfeld, A.M., Florence, M.M., Le Gall, A., Solomonidou, A., Hayes, A.G., Birch, S.P.D., Janssen, M.A., Schurmeier, L., Cornet, T., Ahrens, C., Farr, T.G., the Cassini RADAR Team, 2020. Labyrinth terrain on Titan. Icarus. 344, 113764.

Mandt, K.E., Waite, J.W., Lewis, W., Magee, B., Bell, J., Lunine, J., Mousis, O., Cordier, D., 2009. Isotopic evolution of the major constituents of Titan's atmosphere based on Cassini data. Planet. Space Sci. 57, 1917–1930.

Mandt, K.E., Waite, J.H., Teolis, B., Magee, B.A., Bell, J., Westlake, J.H., Nixon, C.A., Mousis, O., Lunine, J.I., 2012. The $^{12}C/^{13}C$ ratio on Titan from Cassini INMS measurements and implications for the evolution of methane. Astrophys. J. 749, 160.

Matsuno, T., 1966. Quasi-geostrophic motions in the equatorial area. J. Meteor. Soc. Japan 44, 25–43.

McDonald, G.D., Hayes, A.G., Ewing, R.C., Lora, J.M., Newman, C.E., Tokano, T., Lucas, A., Soto, A., Chen, G., 2016. Variations in Titan's dune orientations as a result of orbital forcing. Icarus 270, 197–210.

McKay, C.P., Pollack, J.B., Courtin, R., 1989. The thermal structure of Titan's atmosphere. Icarus 80, 23–53.

McKay, C.P., Pollack, J.B., Courtin, R., 1991. The greenhouse and antigreenhouse effects on Titan. Science 253, 1118–1121.

Mitchell, J.L., 2008. The drying of Titan's dunes: Titan's methane hydrology and its impact on atmospheric circulation. J. Geophys. Res. 113, E08015.
Mitchell, J.L., 2012. Titan's transport-driven methane cycle. Astrophys. J. 756, L26.
Mitchell, J.L., Lora, J.M., 2016. The climate of Titan. Annu. Rev. Earth Planet. Sci. 44, 353–380.
Mitchell, J.L., Pierrehumbert, R.T., Frierson, D.M.W., Caballero, R., 2006. The dynamics behind Titan's methane clouds. Proc. Natl. Acad. Sci. 103, 18421–18426.
Mitchell, J.L., Pierrehumbert, R.T., Frierson, D.M.W., Caballero, R., 2009. The impact of methane thermodynamics on seasonal convection and circulation in a model Titan atmosphere. Icarus 203, 250–264.
Mitchell, J.L., Ádámkovics, M., Caballero, R., Turtle, E.P., 2011. Locally enhanced precipitation organized by planetary-scale waves on Titan. Nat. Geosci. 4, 589–592.
Mitri, G., Meriggiola, R., Hayes, A., Lefevre, A., Tobie, G., Genova, A., Lunine, J.I., Zebker, H., 2014. Shape, topography, gravity anomalies and tidal deformation of Titan. Icarus 236, 169–177.
Muhleman, D.O., Grossman, A.W., Butler, B.J., Slade, M.A., 1990. Radar reflectivity of Titan. Science 25, 975–980.
Neish, C.D., Lorenz, R.D., 2014. Elevation distribution of Titan's craters suggests extensive wetlands. Icarus 228, 27–34.
Neish, C.D., Molaro, J.L., Lora, J.M., Howard, A.D., Kirk, R.L., Schenk, P., Bray, V.J., Lorenz, R.D., 2016. Fluvial erosion as a mechanism for crater modification on Titan. Icarus 270, 114–129.
Newman, C.E., Richardson, M.I., Lian, Y., Lee, C., 2016. Simulating Titan's methane cycle with the TitanWRF general circulation model. Icarus 267, 106–134.
Niemann, H.B., Atreya, S.K., Bauer, S.J., Carignan, G.R., Demick, J.E., Frost, R.L., Gautier, D., Haberman, J.A., Harpold, D.N., Hunten, D.M., Israel, G., Lunine, J.I., Kasprzak, W.T., Owen, T.C., Paulkovich, M., Raulin, F., Raaen, E., Way, S.H., 2005. The abundances of constituents of Titan's atmosphere from the GCMS instrument on the Huygens probe. Nature 438, 779–784.
Niemann, H.B., Atreya, S.K., Demick, J.E., Gautier, D., Haberman, J.A., Harpold, D.N., Kasprzak, W.T., Lunine, J.I., Owen, T.C., Raulin, F., 2010. Composition of Titan's lower atmosphere and simple surface volatiles as measured by the Cassini-Huygens probe gas chromatograph mass spectrometer experiment. J. Geophys. Res. 115, E12006.
Nixon, C.A., Achterberg, R.K., Ádámkovics, M., Bézard, B., Bjoraker, G.L., Cornet, T., Hayes, A.G., Lellouch, E., Lemmon, M.T., López-Puertas, M., Rodriguez, S., Sotin, C., Teanby, N.A., Turtle, E.P., West, R.A., 2016. Titan science with the James Webb Space Telescope. Publ. Astron. Soc. Pac. 128, 018007.
Nixon, C.A., Lorenz, R.D., Achterberg, R.K., Buch, A., Coll, P., Clark, R.N., Courtin, R., Hayes, A., Iess, L., Johnson, R.E., Lopes, R.M.C., Mastrogiuseppe, M., Mandt, K., Mitchell, D.G., Raulin, F., Rymer, A.M., Todd Smith, H., Solomonidou, A., Sotin, C., Strobel, D., Turtle, E.P., Vuitton, V., West, R.A., Yelle, R.V., 2018. Titan's cold case files—Outstanding questions after Cassini-Huygens. Planet. Space Sci. 155, 50–72.
Penteado, P.F., Griffith, C.A., 2010. Ground-based measurements of the methane distribution of Titan. Icarus 206, 345–351.
Perron, J., Lamb, M., Koven, C., Fung, I., Yager, E., Ádámkovics, M., 2006. Valley formation and methane precipitation rates on Titan. J. Geophys. Res. Planet. 111, E11001.
Poggiali, V., Mastrogiuseppe, M., Hayes, A.G., Seu, R., Birch, S.P.D., Lorenz, R., Grima, C., Hofgartner, J.D., 2016. Liquid-filled canyons on Titan. Geophys. Res. Lett. 43, 7887–7894.
Porco, C.C., West, R.A., Squyres, S., McEwen, A., Thomas, P., Murray, C.D., Del Genio, A., Ingersoll, A.P., Johnson, T.V., Neukum, G., Veverka, J., Dones, L., Brahic, A., Burns, J.A., Haemmerle, V., Knowles, B., Dawson, D., Roatsch, T., Beurle, K., Owen, W., 2004. Cassini Imaging Science: Instrument characteristics and anticipated scientific investigations at Saturn. Space Sci. Rev. 115, 363–497.
Porco, C., Baker, E., Barbara, J., Beurle, K., Brahic, A., Burns, J.A., Charnoz, S., Cooper, N., Dawson, D., Del Genio, A., Denk, T., Dones, L., Dyudina, U., Evans, M., Fussner, S., Giese, B., Grazier, K., Helfenstein, P., Ingersoll, A., Jacobson, R.A., Johnson, T., McEwen, A., Murray, C., Neukum, G., Owen, W., Perry, J., Roatsch, T., Spitale, J., Squyres, S., Thomas, P., Tiscareno, M., Turtle, E., Vasavada, A., Veverka, J., Wagner, R., West, R., 2005. Imaging of Titan from the Cassini spacecraft. Nature 434, 159–168.

Radebaugh, J., Lorenz, R.D., Kirk, R.L., Lunine, J.I., Stofan, E.R., Lopes, R.M.C., Wall, S.D., the Cassini Radar Team, 2007. Mountains on Titan observed by Cassini Radar. Icarus 192, 77–91.

Radebaugh, J., Lorenz, R.D., Lunine, J.I., Wall, S.D., Boubin, G., Reffet, E., Kirk, R.L., Lopes, R.M., Stofan, E.R., Soderblom, L., Allison, M., Janssen, M., Paillou, P., Callahan, P., Spencer, C., The Cassini Radar Team, 2008. Dunes on Titan observed by Cassini Radar. Icarus 194, 690–703.

Rafkin, S.C.R., Barth, E.L., 2015. Environmental control of deep convective clouds on Titan: The combined effect of CAPE and wind shear on storm dynamics, morphology, and lifetime. J. Geophys. Res. Planets 120, 739–759.

Rafkin, S.C.R., Soto, A., 2020. Air-sea interactions on Titan: Lake evaporation, atmospheric circulation, and cloud formation. Icarus. 351, 113903.

Rafkin, S., Lora, J.M., Soto, A., Battalio, J.M., 2022. The interaction of deep convection with the general circulation in Titan's atmosphere. part 1: Cloud resolving simulations. Icarus. 373, 114755.

Rannou, P., Montmessin, F., Hourdin, F., Lebonnois, S., 2006. The latitudinal distribution of clouds on Titan. Science 311, 201–205.

Rodriguez, S., Le Mouelic, S., Rannou, P., Sotin, C., Brown, R.H., Barnes, J.W., Griffith, C.A., Burgalat, J., Baines, K.H., Buratti, B.J., Clark, R.N., Nicholson, P.D., 2011. Titan's cloud seasonal activity from winter to spring with Cassini/VIMS. Icarus 216, 89–110.

Rodriguez, S., Le Mouélic, S., Barnes, J.W., Kok, J.F., Rafkin, S.C.R., Lorenz, R.D., Charnay, B., Radebaugh, J., Narteau, C., Cornet, T., Bourgeois, O., Lucas, A., Rannou, P., Griffith, C.A., Coustenis, A., Appéré, T., Hirtzig, M., Sotin, C., Soderblom, J.M., Brown, R.H., Bow, J., Vixie, G., Maltagliati, L., Courrech du Pont, S., Jaumann, R., Stephan, K., Baines, K.H., Buratti, B.J., Clark, R.N., Nicholson, P.D., 2018. Observational evidence for active dust storms on Titan at equinox. Nat. Geosci. 11, 727–732.

Roe, H.G., 2012. Titan's methane weather. Annu. Rev. Earth Planet. Sci. 40, 355–382.

Roe, H.G., de Pater, I., Macintosh, B.A., McKay, C.P., 2002. Titan's clouds from Gemini and Keck adaptive optics imaging. Astrophys. J. 581, 1399–1406.

Roe, H.G., Bouchez, A.H., Trujillo, C.A., Schaller, E.L., Brown, M.E., 2005. Discovery of temperate latitude clouds on Titan. Astrophys. J. 618, L49–L52.

Samuelson, R.E., Nath, N.R., Borysow, A., 1997. Gaseous abundances and methane supersaturation in Titan's troposphere. Planet. Space Sci. 45, 959–980.

Schaller, E.L., Brown, M.E., Roe, H.G., Bouchez, A.H., 2006a. A large cloud outburst at Titan's south pole. Icarus 182, 224–229.

Schaller, E.L., Brown, M.E., Roe, H.G., Bouchez, A.H., Trujillo, C.A., 2006b. Dissipation of Titan's south polar clouds. Icarus 184, 517–523.

Schaller, E.L., Roe, H.G., Schneider, T., Brown, M.E., 2009. Storms in the tropics of Titan. Nature 460, 873–875.

Schinder, P.J., Flasar, F.M., Marouf, E.A., French, R.G., McGhee, C.A., Kliore, A.J., Rappaport, N.J., Barbinis, E., Fleischman, D., Anabtawi, A., 2011. The structure of Titan's atmosphere from Cassini radio occultations. Icarus 215, 460–474.

Schinder, P.J., Flasar, F.M., Marouf, E.A., French, R.G., McGhee, C.A., Kliore, A.J., Rappaport, N.J., Barbinis, E., Fleischman, D., Anabtawi, A., 2012. The structure of Titan's atmosphere from Cassini radio occultations: Occultations from the Prime and Equinox missions. Icarus 221, 1020–1031.

Schinder, P.J., Flasar, F.M., Marouf, E.A., French, R.G., Anabtawi, A., Barbinis, E., Fleischman, D., Achterberg, R.K., 2020. The structure of Titan's atmosphere from Cassini radio occultations: One- and two-way occultations. Icarus. 345, 113720.

Schneider, T., Graves, S.D.B., Schaller, E.L., Brown, M.E., 2012. Polar methane accumulation and rainstorms on Titan from simulations of the methane cycle. Nature 481, 58–61.

Schröder, S., Karkoschka, E., Lorenz, R., 2012. Bouncing on Titan: Motion of the Huygens probe in the seconds after landing. Planet. Space Sci. 73, 327–340.

Smith, R.B., 2019. 100 years of progress on mountain meteorology research. Meteorol. Monogr. 59, 20.1–20.73.

Smith, P.H., Lemmon, M.T., Lorenz, R.D., Sromovsky, L.A., Caldwell, J., Allison, M.D., 1996. Titan's surface, revealed by HST imaging. Icarus 119, 336–349.

Smith, C.L., Cooper, B.A., Moores, J.E., 2016. Possible ground fog detection from SLI imagery of Titan. Icarus 271, 269–278.
Sobel, A.H., Nilsson, J., Polvani, L.M., 2001. The weak temperature gradient approximation and balanced tropical moisture waves. J. Atmos. Sci. 58, 3650–3665.
Stephan, K., Jaumann, R., Brown, R.H., Soderblom, J.M., Soderblom, L.A., Barnes, J.W., Sotin, C., Griffith, C.A., Kirk, R.L., Baines, K.H., Buratti, B.J., 2010. Specular reflection on Titan: liquids in Kraken Mare. Geophys. Res. Lett. 37, L07104.
Stevenson, D.J., Potter, B.E., 1986. Titan's latitudinal temperature distribution and seasonal cycle. Geophys. Res. Lett. 13, 93–96.
Stofan, E.R., Elachi, C., Lunine, J.I., Lorenz, R.D., Stiles, B., Mitchell, K.L., Ostro, S., Soderblom, L., Wood, C., Zebker, H., Wall, S., Janssen, M., Kirk, R., Lopes, R., Paganelli, F., Radebaugh, J., Wye, L., Anderson, Y., Allison, M., Boehmer, R., Callahan, P., Encrenaz, P., Flamini, E., Francescetti, G., Gim, Y., Hamilton, G., Hensley, S., Johnson, W.T.K., Kelleher, K., Muhleman, D., Paillou, P., Picardi, G., Posa, F., Roth, L., Seu, R., Shaffer, S., Vetrella, S., West, R., 2007. The lakes of Titan. Nature 445, 61–64.
Strobel, D.F., 1974. The photochemistry of hydrocarbons in the atmosphere of Titan. Icarus 21, 466–470.
Strobel, D.F., Atreya, S.K., Bézard, B., Ferri, F., Flasar, F.M., Fulchignoni, M., Lellouch, E., Müller-Wodarg, I., 2009. Atmospheric structure and composition. In: Brown, R.H., Lebreton, J.-P., Waite, J.H. (Eds.), Titan from Cassini-Huygens. Springer, pp. 235–257.
Tan, S., Kargel, J.S., Giles, M.M., 2013. Titan's atmosphere and surface liquid: New calculation using statistical associating fluid theory. Icarus 222, 52–73.
Teanby, N.A., Sylvestre, M., Sharkey, J., Nixon, C.A., Vinatier, S., Irwin, P.G.J., 2019. Seasonal evolution of Titan's stratosphere during the Cassini mission. Geophys. Res. Lett. 46, 3079–3089.
Tobie, G., Lunine, J.I., Sotin, C., 2006. Episodic outgassing as the origin of atmospheric methane on Titan. Nature 440, 61–64.
Tokano, T., 2005. Meteorological assessment of the surface temperatures on Titan: constraints on the surface type. Icarus 173, 222–242.
Tokano, T., 2008. Dune-forming winds on Titan and the influence of topography. Icarus 194, 243–262.
Tokano, T., 2009. Impact of seas/lakes on polar meteorology of Titan: Simulation by a coupled GCM-Sea model. Icarus 204, 619–636.
Tokano, T., 2010. Relevance of fast westerlies at equinox for the eastward elongation of Titan's dunes. Aeolian Res. 2, 113–127.
Tokano, T., 2019. Orbitally and geographically caused seasonal asymmetry in Titan's tropospheric climate and its implications for the lake distribution. Icarus 317, 337–353.
Tokano, T., Lorenz, R.D., 2021. Paleoclimate evolution on Titan after episodic massive methane outgassing simulated by a global climate model. J. Geophys. Res. Planets. 126, e2021JE007081.
Tokano, T., McKay, C.P., Neubauer, F.M., Atreya, S.K., Ferri, F., Fulchignoni, M., Niemann, H.B., 2006. Methane drizzle on Titan. Nature 442, 432–435.
Tomasko, M.G., Archinal, B., Becker, T., Bézard, B., Bushroe, M., Combes, M., Cook, D., Coustenis, A., de Bergh, C., Dafoe, L.E., Doose, L., Douté, S., Eibl, A., Engel, S., Gliem, F., Grieger, B., Holso, K., Howington-Kraus, E., Karkoschka, E., Keller, H.U., Kirk, R., Kramm, R., Küppers, M., Lanagan, P., Lellouch, E., Lemmon, M., Lunine, J., McFarlane, E., Moores, J., Prout, G.M., Rizk, B., Rosiek, M., Rueffer, P., Schröder, S.E., Schmitt, B., See, C., Smith, P., Soderblom, L., Thomas, N., West, R., 2005. Rain, winds and haze during the Huygens probe's descent to Titan's surface. Nature 438, 765–778.
Toon, O.B., McKay, C.P., Courtin, R., Ackerman, T.P., 1988. Methane rain on Titan. Icarus 75, 255–284.
Turtle, E.P., Perry, J.E., McEwen, A.S., Del Genio, A.D., Barbara, J., West, R.A., Dawson, D.D., Porco, C.C., 2009. Cassini imaging of Titan's high-latitude lakes, clouds, and south-polar surface changes. Geophys. Res. Lett. 36, L02204.
Turtle, E.P., Del Genio, A.D., Barbara, J.M., Perry, J.E., Schaller, E.L., McEwen, A.S., West, R.A., Ray, T.L., 2011a. Seasonal changes in Titan's meteorology. Geophys. Res. Lett. 38, L03203.

Turtle, E.P., Perry, J.E., Hayes, A.G., Lorenz, R.D., Barnes, J.W., McEwen, A.S., West, R.A., Del Genio, A.D., Barbara, J.M., Lunine, J.I., Schaller, E.L., Ray, T.L., Lopes, R.M.C., Stofan, E.R., 2011b. Rapid and extensive surface changes near Titan's equator: Evidence of April showers. Science 331, 1414–1417.

Turtle, E.P., Perry, J.E., Hayes, A.G., McEwen, A.S., 2011c. Shoreline retreat at Titan's Ontario Lacus and Arrakis Planitia from Cassini Imaging Science Subsystem observations. Icarus 212, 957–959.

Turtle, E.P., Perry, J.E., Barbara, J.M., Del Genio, A.D., Rodriguez, S., Sotin, C., Lora, J.M., Faulk, S., Corlies, P., Kelland, J., MacKenzie, S.M., West, R.A., McEwen, A.S., Lunine, J.I., Pitesky, J., Ray, T.L., Roy, M., 2018. Titan's meteorology over the Cassini mission: Evidence for extensive subsurface methane reservoirs. Geophys. Res. Lett. 45, 5320–5328.

Vinatier, S., Bézard, B., Lebonnois, S., Teanby, N.A., Achterberg, R.K., Gorius, N., Mamoutkine, A., Guandique, E., Jolly, A., Jennings, D.E., Flasar, F.M., 2015. Seasonal variations in Titan's middle atmosphere during the northern spring derived from Cassini/CIRS observations. Icarus 250, 95–115.

Wong, M.L., Yung, Y.L., Gladstone, G.R., 2015. Pluto's implications for a snowball Titan. Icarus 246, 192–196.

Wye, L.C., Zebker, H.A., Lorenz, R.D., 2009. Smoothness of Titan's Ontario Lacus: Constraints from Cassini RADAR specular reflection data. Geophys. Res. Lett. 36, L16201.

Yung, Y., Allen, M., Pinto, J.P., 1984. Photochemistry of the atmosphere of Titan: Comparison between model and observations. Astrophys. J. Suppl. Ser. 55, 465–506.

Zebker, H., Hayes, A., Janssen, M., Le Gall, A., Lorenz, R., Wye, L., 2014. Surface of Ligeia Mare, Titan, from Cassini altimeter and radiometer analysis. Geophys. Res. Lett. 41, 308–313.